Department of Precision and Microsystems Engineering

Design of a Flapping Wing for Application in a Micro Air Vehicle

Anirudh Narayanan

Report no : 2019.035
Coach : Dr.ir. J.F.L. Goosen
Professor : Prof.dr.ir. A. van Keulen
Specialisation : Engineering Mechanics
Type of report : Master of Science Thesis
Date : 17 September 2019

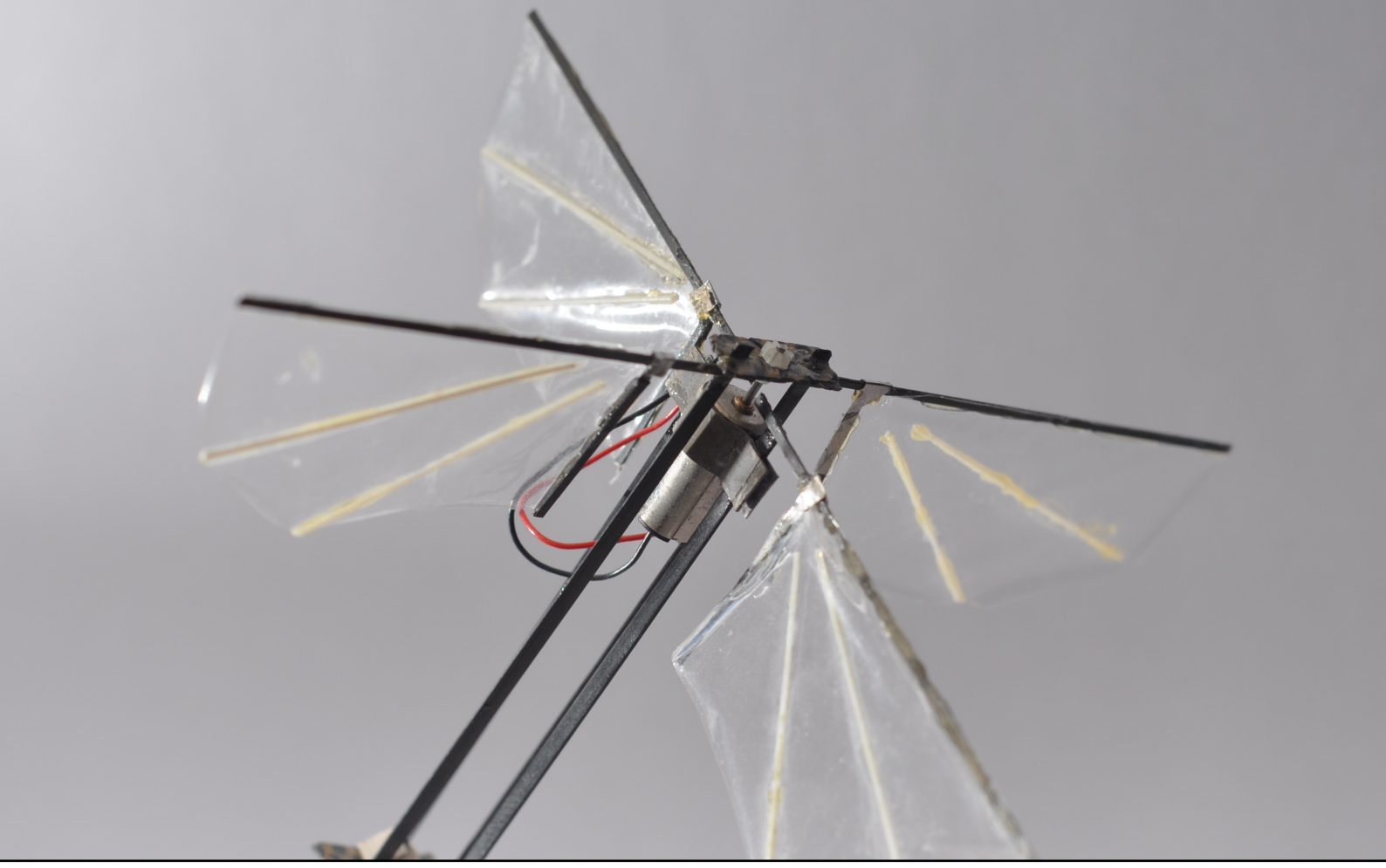

TU Delft Delft University of Technology

Challenge the future

Design of a Flapping Wing
Application in a Micro Air Vehicle

Master of Science Thesis

For the degree of Master of Science in High Tech Engineering at Delft University of Technology

Anirudh Narayanan

September 17, 2019

Faculty of Mechanical, Maritime and Materials Engineering (3mE) · Delft University of Technology

Abstract

The goal of this study is to understand the processes and wing characteristics that influence lift generation of a flapping wing, and apply the acquired knowledge in an optimization setting to obtain an optimal wing thickness distribution which maximizes effective wing lift. To achieve this, an extensive literature survey was conducted to identify geometrical characteristics of the wing that are known to help maximize wing lift, and loading conditions under which a given wing design must be numerically studied. Additionally, a cubic pressure load distribution was developed to approximately mimic the aerodynamic pressure acting on the surface of the wing. Changes were made to the research code, *Charles*, to achieve some of the desired features. Using some of the identified parameters and load cases, an optimization problem was formulated and thickness distributions were obtained for two wing planform shapes with uniform initial thicknesses. The optimized rectangular wing planform achieved an angle of attack of 43.15 deg at the wing tip under high magnitude inertial loads whereas the hawkmoth wing shape achieved an angle of 39.81 deg at 60% of the wing span under the same load. The results were compared and discussed for different load cases, and general patterns were identified which give insight on flapping wing design.

Table of Contents

List of Figures

Preface

During the introduction week of my Masters program at Delft University of Technology, I attended a presentation on the Atalanta project - a Flapping Wing Micro Air Vehicle with certain novel characteristics. I was fascinated by the project and approached Dr.ir. J.F.L. Goosen to see if there were any structural mechanics or optimization related projects associated with the Atalanta bug. When he informed me about the wing design project, I was initially anxious due to the vast scope of the project. However, my passion for the research area and my fascination with the tiny drone convinced me to take the plunge.

I would like to thank my supervisor, Dr.ir. J.F.L. Goosen, for all the support, advice, and feedback he gave me throughout the duration of the project. I would also like to thank Prof.dr.ir. A. Van Keulen for his assistance and guidance. Without his help, I would not have understood the workings of research code "Charles" well enough to implement and test the features I desired. Finally, I would like to thank Lidan Zhang and Max Van Der Kolk for their technical support and advice.

Delft University of Technology
September 17, 2019

Anirudh Narayanan

To my parents and friends.

"To invent an airplane is nothing. To build one is something. To fly is everything."
— *Otto Lilienthal*

Chapter 1

Introduction

This chapter aims to provide a basic overview of the history of flapping wing flight and also shed light on more recent developments in the field. The important role of tiny, autonomous drones in the future is described and the applications of Flapping Wing Micro Air Vehicles (FWMAVs) are listed. A short description of the Atalanta project, of which this study is a part, is given and certain key characteristics of the Atalanta bug are showcased. Finally, a summary of the unsteady aerodynamic phenomena that govern flapping flight is given.

1-1 Flapping Wing History

Throughout history, scientists and engineers have been deeply fascinated with the flight of birds, insects and even bats. Probably the most famously recognized documented instance of this fascination is the ornithopter design drawn in detail by Leonardo da Vinci in 1485 [3]. What set apart da Vinci's design from previous attempts was that the machine would be able to carry a human being while also being powered by the person. After da Vinci, however, not much progress was made in flapping wing aviation until the 19th century [3].

In the 17th century, Italian physicist Giovanni Borelli published his famous book *De Motu Animalium* detailing the flapping wing flight of birds. He showcased his understanding of the complex aerodynamics through sketches of birds changing horizontal direction (i.e., yawing) by beating one wing at a different rate than the other. The observations made by Borelli were similar to those made by da Vinci earlier and were important contributions to understanding the mechanics of avian flight.

In 1902, Edward Frost built an ornithopter using materials like willow, silk, and feathers [4]. Although his designs imitated the the appearance of birds, the contraption was too heavy to achieve lift. Belgian engineer Adhemar de la Hault built a very complex machine that would imitate the flight of birds. Historical records show [5] that in 1908 his invention was able to lift off the ground for a moment. However, it appears that subsequent experiments fell prey to the machine's mechanical part failures.

In recent times, many projects involving flapping wing drones have been launched and realised such as the Phoenix bird [6] which is a larger bird-like ornithopter capable of carrying payloads of approximately 400 g, and the Harvard Robotic Fly [7] which is a biologically inspired at-scale insect drone weighing a mere 60 mg. The Delfly project [8] resulted in a 3.07 g FWMAV with an optic-flow based control implementation, and the ongoing Atalanta project under which this thesis project was carried out, utilizes a chemical-based actuator which is posed to provide efficiency advantages.

Insect-like microbots, initially developed for defense and espionage purposes, have vast applications in fields ranging from farming to topographical mapping operations [9]. For instance, a swarm of Micro air vehicles (MAVs) could be used to transport items between places, spray pesticide over large swathes of farmland, aid in survey for conducting rescue operations, inspect structures for preventative maintenance, and even enter areas hazardous to humans. The future of humanity is closely linked with the development of such robots which can aid in day-to-day activities. Given the nascent nature of this technology, there is still a lot of research to be done in the field. One of these research areas is the design of a wing for application in Flapping Wing Micro Air Vehicles (FWMAVs), which is what this project is focused on.

1-2 Key Aspects of Flapping Wing Flight

The fundamental difference between fixed and flapping wing lift generation is derived from the aerodynamic phenomena harnessed by them. Fixed wings use steady mechanisms to achieve lift whereas flapping wings use unsteady mechanisms such as wake capture, leading edge vortices, and circulation effects [10, 11, 12] to produce lift. These effects are discussed in further detail in subsequent chapters. One argument is that these effects harnessed by flapping wings leads to energy being wasted in generating vortices in the wake of the wing [13]. However, studies [1] have shown that the scaled propulsive efficiency of flapping wings are higher than fixed wing counterparts. The ability of flapping wings to achieve reduced power consumption at low cruising speeds [1] and hover conditions results in better maneuverability and efficiency in confined spaces.

The graphs in Fig 1-1 illustrate the important advantage that flapping wing flight holds. However, the comparison was made between living organisms that have evolved over millenia to be as efficient as possible, and man-made fixed wing based transportation technology. Therefore, truly realising the advantages offered by flapping flight requires much more research and study. When it comes to insect flight, certain aspects can already be mimicked with a lot of success. For instance, hovering insects often exhibit a symmetric, periodic back and forth wing motion [14]. Such a motion could be replicated by resonant mechanisms such as the compliant mechanism developed by Bolsman et al [15]. The advantage of utilizing resonance is that the same motion can be produced while having lower power consumption.

For long range, higher speed flights, fixed wings still hold a significant advantage as compared to flapping wings. The maximum lift-to-drag ratios noted for birds and other natural flappers were lower than those of scaled down aircraft [1]. This may be due to higher induced drag effects for flapping flight which is caused due to a non-linear interaction of the wing surface with the surrounding wake. At smaller scales, fixed wing flight requires higher velocities to

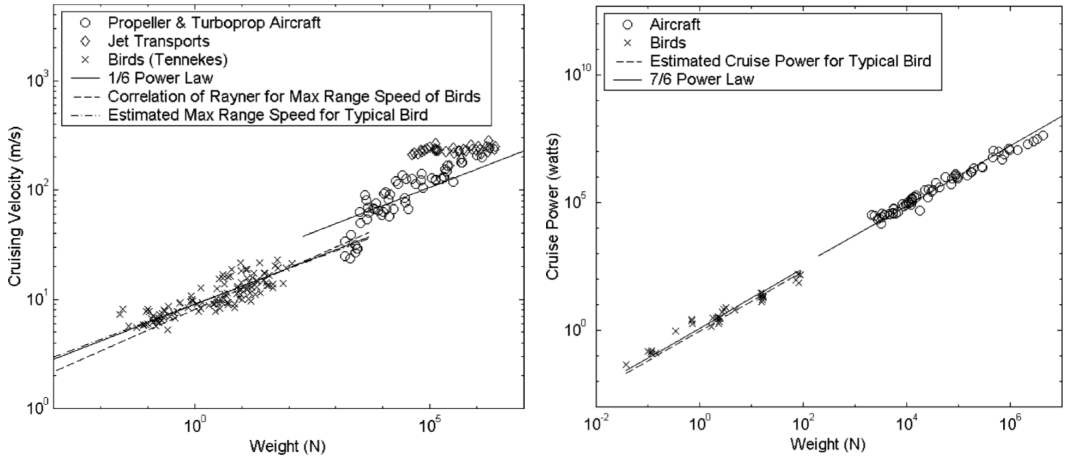

(a) Scaled cruise velocity **(b)** Scaled cruise power

Figure 1-1: A comparison between fixed wing and flapping wing flight based on scaled parameters conducted by Liu et al [1] shows how the cruise velocity and power relate to the scaled weight of each of the systems studied. The low cruising velocity combined with reduced cruise power makes flapping wing flight highly advantageous in confined space situations.

maintain the required lift. This is due to the high induced flow required over the wings. Thus, although fixed wing and rotary wing MAVs have become ubiquitous in recent times, there is significant merit to studying flapping wing flight.

1-3 Atalanta Project

The Atalanta project, kickstarted under the Devlab group, aims to build a mechatronic bug which can fly in different environments and be completely self-supporting in terms of energy consumption and navigation. It uses a novel chemical-based actuator that poses a lot of advantages and an optic flow based control system. The prototype bug shown [15] in Fig 1-2 is designed with a wingspan of 100 mm and a maximum combined load of 4 g.

Some aspects of the Atlanta bug have been worked on and these have been mentioned below.

- **Actuator:** Conventional motors exhibit various issues like reduced power density when scaled down. Hence, the Atalanta project is driven by a hydrogen peroxide based actuator which harnesses chemical energy [16] to power the bug. A key characteristic of this is that the weight of the bug decreases as the fuel is consumed.
- **Drive Mechanism:** The insect thorax constitutes the power source and drives the movement of the wings in an elastic manner. Some insects use resonance to help reduce the inertial cost of wing movement and thereby decrease energy consumption. Thus, the drive mechanism can be seen as a tuned spring-mass-damper system. Different drive mechanisms were designed using compliant elements [15] to simulate the behavior of the insect thorax to achieve a similar result.

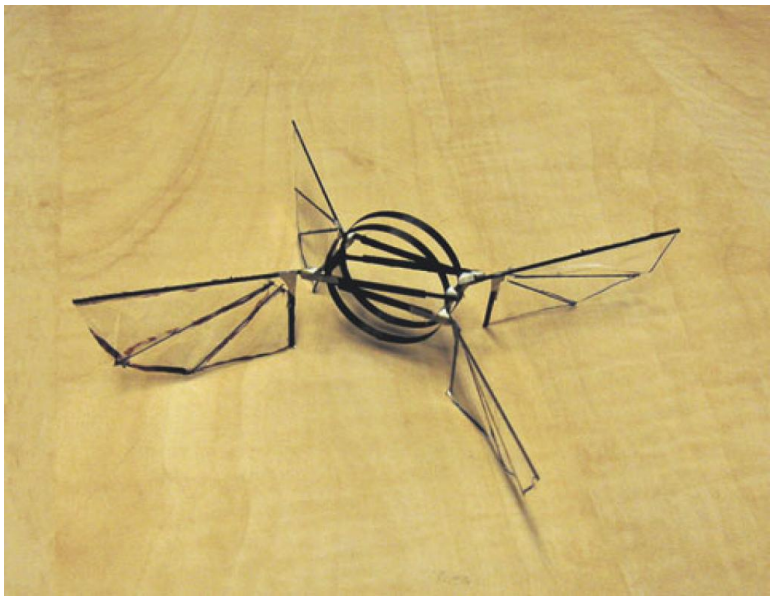

Figure 1-2: Designed by Bolsman [15], the Atalanta drone uses compliant mechanisms to achieve insect thorax-wing resonance thereby driving wing movement. Photo obtained from [15].

- **Flight Navigation:** There are two aspects that are tackled under navigation.
  - *Sensing* - Standard image processing and data transmission electronics would add excessive weight due to the large number of onboard components required. Hence, a novel optic flow based sensing method was developed [17] which allowed for usage of a lightweight six optic sensor.
  - *Control* - The compliant mechanisms and elements used by the Atalanta team for the drive mechanism needed a new way to actively manipulate those components in order to achieve directional control. The approach used was to control the wing kinematics by tuning the local structural properties of the wing. The feasibility of various methods was tested and it was concluded that piezoelectric polymers and electrostatic softeners could theoretically be used [18] to realize the required property changes.
- **Wing Design:** In order to design flapping wings, a quasi-steady model was developed by Wang et al [19] that attempts to describe the unsteady aerodynamic effects experienced by the wing without using many empirical parameters. The results from this model are used to generate loads for optimization studies, which are described in subsequent chapters.

1-4 Governing Aerodynamic Mechanisms

Understanding the unsteady aerodynamic processes and how they interact with each other to produce lift is a necessary step before a flapping wing can be designed. The interaction between the wing and the surrounding fluid is highly complex and the timing of these interactions has significant impact on the lift generated. The flow around the wings of insects is

generally unsteady and incompressible and is characterized by intermediate Reynold's numbers [15]. Conventional steady-state theory fails when it comes to explaining the high forces produced by flapping wings [11]. Some of the essential unsteady aerodynamic mechanisms that significantly affect lift and thrust production in flapping wings are listed below.

- *Leading Edge Vortex:* When the wing moves through the surrounding fluid, a stable, expanding vortex [10, 12] is generated at the leading edge of the wing. This vortex is formed on top of the wing and has high rotation leading to high velocities. The high velocity leads to a pressure differential which results in a low pressure region on the wing surface. The presence of this low pressure region on the wing surface results in the generation of lift. Once the vortex is shed, the lift also drops in a similar manner. The LEV is stable for a large range of flying insects.

- *Rotational Circulation:* This effect is present only during stroke reversal. During stroke reversal, the rotational velocities are large; There are some vortices generated and shed when the wing rotates and the wing must then interact with the flow field induced by these vortices. By varying the wing rotation timing (e.g., when the wing flips from pronated to supinated) the lift generated can be tuned. The effect is very similar to the Magnus effect, which makes a spinning ball curve from it's path. If the wing flips before direction reversal, lift is produced [11]. On the other hand, if the wing flips after reversing direction, then a downward force is generated.

- *Wake Capture:* The flow generated during a stroke can increase the surrounding fluid velocity at the start of the next stroke and thus potentially increase the lift force generated in the subsequent strokes. There are also vortices shed during a stroke that the wing surface interacts with during the succeeding stroke resulting in elevated drag forces at the start of each translational stroke. The wake capture effect is most pronounced during the stroke reversal phase of the motion. Although the timing of wake capture is constant on average, the magnitude and direction can be varied. If wing rotation occurs before stroke reversal, positive lift is generated. However, if the wing flips after stroke reversal, the wing intercepts its own wake at an angle that produces negative lift [11].

- *Clap and Fling:* There are additional mechanisms that have been identified like the clap and fling effect [14, 20]. Towards the end of the upstroke, the wings go further and touch each other above the insect body in a clapping motion. This is followed by a downstroke in which the wings are rolled open rapidly. It is theorized that this effect kickstarts the formation of leading edge vortices which helps generate lift for insects with smaller wing strokes. There are other interpretations which suggest [21] that the wings touching could also be a consequence of the insect maximizing the space swept by the wing thereby generating more lift.

- *Added Mass Effects:* Another effect identified is that of the influence of surrounding fluid viscosity on the wing kinematics. The fluid in the immediate vicinity of the wing is affected by the rapid acceleration and deceleration of the wing. The viscosity of this fluid influences the area around the wing and the surrounding fluid moves along with the wing acting as an added mass [22]. This "virtual mass" adds to the effective inertia of the wing and its magnitude is sometimes comparable to the mass of the wing itself.

A crucial realization is that the above described mechanisms interact and influence each other in an intricate manner. For instance, when timed correctly, the wake capture force increases following a prominent rotational circulation effect [11]. This highlights how insects are able to harness the energy of the wake generated by their own movement. An insect has the ability of recovering energy that it lost during the previous stroke from its surroundings, greatly improving the efficiency of force production. If we are to replicate the energy efficiency of insect flight, we need to be able to model the unsteady phenomena that govern it with reasonable accuracy. This was done by Wang et al [19], and the results from this model are used in this study.

Chapter 2

Wing Design Methodology

In this chapter, different approaches for modelling the unsteady aerodynamic mechanisms governing flapping flight are discussed, and their advantages listed. The quasi-steady aerodynamic model developed by Wang et al [19] is described. A flapping wing's geometrical characteristics and the unique form of loading which it experiences are detailed and the implications for an optimization study are analysed. A few of the software options available to conduct such a study are briefly mentioned. Finally, research questions are formulated for the thesis project.

2-1 Modelling of Aerodynamic Phenomena

The design of flapping wings for FWMAVs is a complicated subject. Insect wings have evolved over millions of years to perform a specific task or action efficiently. Consider the wings of a butterfly, a dragonfly and a common housefly; It is apparent that the wings of each of these creatures is perfectly suited for their unique activities. Therefore, it is understandable that the analytical modelling of wings that take into account the diverse flapping kinematics and dynamics is a necessary task. Much work has been done to understand and model the aerodynamics that govern flapping flight. There are three major modelling approaches, namely - steady-state, quasi-steady, and unsteady models.

Steady-state models Steady-state models do not account for transient forces that occur during the stroke of the wing and instead give us an idea of the average force production of flapping flight. Steady-state models tend to overestimate the average lift produced and fail to make accurate predictions in most cases. This is due to the fact that they do not account for transient drag forces which are high when the wing undergoes stroke reversal.

Quasi-steady models Quasi-steady models generally leverage experimental results and incorporate empirical parameters in the model to more accurately predict flight performance. This does result in accurate predictions of stroke-averaged values for mean lift production.

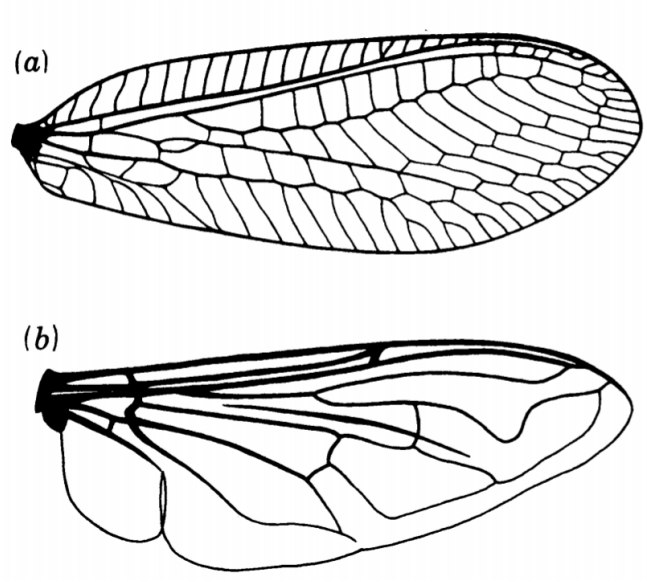

Figure 2-1: A study conducted by Ellington et al [23] compares the wings of the (a) green lacewing (*Chrysopa carnea*) and the (b) drone-fly (*Eristalis tenax*). The wing of the drone-fly has fewer venations than the lacewing. It can also be seen that the shape of the wing planform differs in subtle ways.

However, many of them fail to capture the transient peaks in drag and lift accurately and generally underestimate the mean drag coefficient [24]. A limitation of many existing quasi-steady models is that the wing pitching motion of insects is generally not incorporated, while it is known [25, 26] that for steady-state flying or hovering, the wing pitching is passive.

An additional limitation is that of accurately modelling coupling effects. Recent work by Whitney and Wood [27] proposes a quasi-steady model that includes aerodynamic loads due to wing rotation and translation, and also incorporates the added virtual mass effect through the use of empirical parameters. However, the coupling effect between the translational load and the rotational load was not included in their study. Experiments show [22] that the coupling effect and the pitching motion of the wing are of high importance and significantly affect the loads generated by the flapping wings. Thus, it is necessary to include both of these effects in a quasi-steady model. The dependence of many of these models on empirical parameters limits their application to general flapping wing analyses.

Unsteady models Finally, unsteady models attempt to model the unsteady flow phenomena without actually conducting numerical simulations that directly solve the complex Navier-Stokes equations. Although these models are successful in modelling the changing flow field during flapping flight, they are computationally very expensive and carrying out optimization studies using such models would require a lot of processing power. The Kutta condition states that the circulation for a body with a sharp trailing edge travelling through a fluid adjusts itself so that the rear stagnation point holds itself at the sharp end of the trailing edge. This condition is usually employed and satisfied [28] by most unsteady models. This condition holds true when there is minimal wing pitch reversal however, during stroke reversals of a flapping wing, the pitch maneuvers in such a manner that the fluid flows around the trailing

edge rather than along it, questioning the applicability [28] of the Kutta condition.

2-2 Wing Nomenclature

Some basic nomenclature for a simple rectangular wing is shown in Fig 2-2. The spanwise and chordwise directions are used to describe various geometrical properties of the wing.

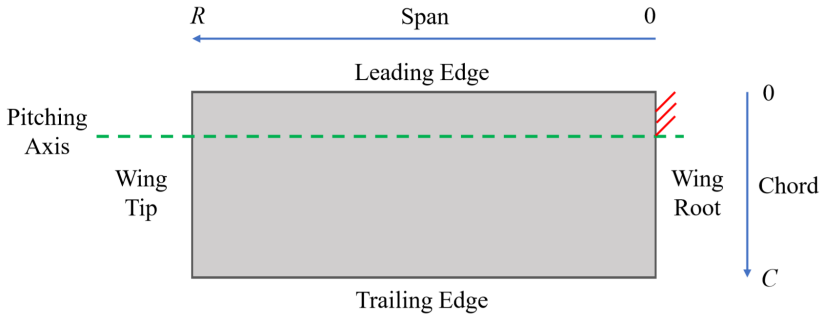

Figure 2-2: The standard nomenclature for different parts of the wing is shown here. Spanwise directions usually indicate aspects of the wing in-plane with the wing planform like the shape of the wing. Chordwise descriptions usually indicate cross-sectional attributes of the wing along the chord direction.

For instance, the shape of the wing planform is described by the Spanwise Area Distribution (SWAD). The shape of the wing may be characterized differently depending on the type of wing. For instance, a Beta probability density function may be used to attain the shape of a hawkmoth wing [23]. The Chordwise Area Distribution (CWAD), on the other hand, describes the shape of the wing cross section. Similarly, the Spanwise Mass Distribution (SWMD) and the Chordwise Mass Distribution (CWMD) are also useful functions to describe wing morphology. The rotation of the wing about an axis parallel to the chordwise direction is called *sweeping* and the rotation of the wing about an axis parallel to the spanwise direction is called *pitching*. The sweeping axis in this study, passes through the wing root. Pitching of the wing allows it to attain a certain angle of attack and this angle has a large influence on the amount of lift generated. The above-mentioned terminology is used extensively throughout the report.

2-3 Existing Quasi-Steady Aerodynamic Model

It is clear from the previous section that the best option would be to opt for a quasi-steady aerodynamic model which does not have a heavy dependence on empirical parameters. Wang et al [19] developed an analytical quasi-steady model for flapping wings that aims to quickly evaluate the aerodynamic performance of a given wing design. In this model, the flow is assumed to be incompressible and the flapping wing is modelled as a series of rigid chordwise strips as shown in Fig 2-3. This allows for simplification of the aerodynamic pressure load into a point force for each chord.

The model was then used to carry out optimization studies of certain aspects of the wing geometry such as the wing root stiffness, the young's modulus of the wing, and pitching axis

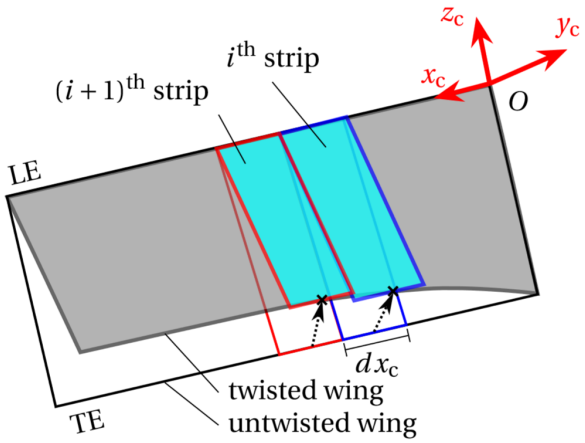

Figure 2-3: Blade element method used by Wang et al[2] assumes each infinitesimal chordwise strip to be rigid. This allows for simplifcation of the force distribution and easier analytical modelling of the wing twist.

orientation. However, these optimization studies were carried out by decoupling different behavioural aspects of the wing. For instance, the root stiffness of the wing was decoupled from the rest of the wing's stiffness. This allowed for an optimized root stiffness that could be achieved by means of a torsional spring at the wing root. The study also looks at different wing SWADs and compares their performance, resulting in the observation that the hawkmoth wing profile with an optimized pitching axis location results in the largest effective lift as compared to other wing shapes. The CWAD was also studied by using a function to describe a kite profile for the CWAD and comparing it with a uniform CWAD. A similar approach was used for the mass distribution in the chordwise and spanwise directions wherein a function was used to describe different profiles but none of these aspects were optimized.

The geometric aspects of the wing that were optimized, such as the pitching axis orientation, are taken into account as parameters for wing design evaluation which is described in the review paper included in this report as Chapter 3.

2-4 Design Optimization Approach

The aim of this study is to optimize certain aspects of the wing in order to maximize its lift production. as the wing performs a flapping stroke, it experiences high inertial surface loads and also aerodynamic pressure loads. Under these changing load conditions, the wing needs to be able to remain stiff so as to harness the transient forces, while at the same time maintaining a certain angle of attack at the tip. Lift-maximizing angles of attack are known to be between 30 and 45 degrees at the wing tip.

Essentially, a wing design needs to be optimized such that under certain load cases, the wing is stiff in bending but is still able to twist. For the purpose of this study, the shape of the wing planform is kept constant. The factors that can be tuned in this study are thus - the chordwise area and mass distributions, and the spanwise mass distribution. All of these parameters are linked to the thickness distribution of the wing. Rather than use each of them as separate

design variables, the design variable is instead chosen to be the thickness of each element as this simplifies the problem considerably. Hence, the aim is to obtain a thickness distribution that satisfies certain constraints to achieve high bending stiffness under applied loads, while having a lower rotational stiffness to maintain the angle of attack.

When it comes to the applied loads, the aerodynamic model developed by Wang et al [19] assumes rigidity in the chordwise strips and this allows for the pressure distribution along the chord direction to be simplified into a point load acting at a certain center of pressure along each chordwise strip. Thus, the aerodynamic pressure load was converted to a simpler force distribution along a line from the wing root to the tip. This approximation is no longer valid for the current study as the entire structure is modelled to be flexible. Hence, a process was developed to design a surface load which is a reasonable approximation of the actual aerodynamic load. This has been described extensively in Chapter 3.

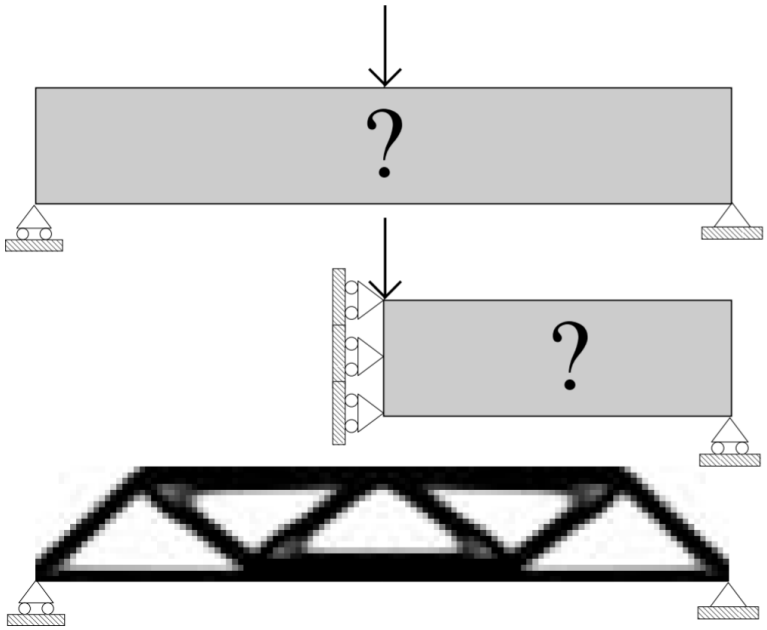

Figure 2-4: The material distribution of a simply supported beam is optimized using the 99 lines of code published by Sigmund [29]. As can be seen, the penalization exponent is set such that the resulting design is black-white, i.e., there are no areas with grey/intermediate material.

Optimization problems like these are usually carried out using the SIMP (Solid Isotropic Material with Penalization) approach. This uses a penalized pseudo-density term for each element on the structure which encourages the optimizer to achieve a solid-void type design as shown in Fig 2-4. An option considered was to use a similar approach and implement a pseudo-thickness for each element but the deformation profile of the current problem is highly nuanced. The wing is expected to twist and stretch under the applied loads, which means that this problem involves membrane and bending deformations. Further, the slender nature of the structure, indicated by the high chord to thickness ratio, means that the membrane forces that the wing would experience under such loading conditions would not be insignificant as membrane action tends to take over with reducing thickness. More details on the optimization approach for the wing design problem are given in Chapter 4, which presents a technical paper.

Available Software Solutions Certain software solutions such as COMSOL and Altair OptiStruct are capable of performing thickness distribution optimization using their shape optimization framework. However, their applicability for slender structures experiencing complicated loads hasn't been tested.

Research Questions Based on the above, a set of research questions was established and is listed below.

- How can we evaluate and qualitatively compare one wing design from another for application in a Flapping Wing Micro Air Vehicle?
  - Which phases of the flapping stroke are the most critical to study with respect to wing lift generation?
  - Once critical phases of the flapping stroke have been identified, what evaluation parameters can be used to compare generic wing designs?
- Can we set up an optimization algorithm that outputs an optimal thickness distribution for a wing?
  - How do we implement sensitivities for thickness distribution optimization of extremely slender structures?
  - Can the selected critical load cases be used in combination with some of the evaluation parameters to formulate a wing design optimization problem?

To answer the above research questions, two papers were written. The first paper, which is a review paper, addresses the first main research question based on evaluation and comparison of existing wing designs. A second technical paper leverages the load cases and parameters identified during the review to formulate an optimization problem that outputs thickness distributions on a given wing shape under certain loading conditions.

Chapter 3

Review Paper

This chapter preents a review paper that was written as a part of the thesis project. The paper aims to identify parameters that influence lift generation of a flapping wing to enable qualitative comparisons for general wing designs. Additionally, given the sensitivity of the wing to loading conditions, an aerodynamic load surface was developed to apply a required net force on the wing. Finally, different phases of a flapping stroke cycle are compared and key regions of the stroke are highlighted as load cases for wing evaluation.

A Simple Qualitative Review and Evaluation of Flapping Wing Design

A. Narayanan, Dr. ir. J.F.L. Goosen and Prof. dr. ir. A. van Keulen

ARTICLE INFO

Keywords:
flapping wing
design
lift generation
load cases

ABSTRACT

This study looks at the design of a flapping wing for use in micro-air vehicles from a qualitative perspective. The different existing aerodynamic models used to predict lift generation of flapping wings are briefly discussed, followed by a detailed look at the geometric factors that influence lift generation. The importance of correctly modelling slender flapping wings by including membrane deformations is decribed and the triangular shell element developed by Keulen et al [20] is highlighted as it satisfies these requirements. Finally, load cases are defined which can be used to evaluate a given wing design using a set of parameters.

1. Introduction

The last few years have seen a significant uptick [9] in the number of autonomous robots and drones. These drones, initially focused towards defense and espionage purposes, have vast applications in fields ranging from farming to topographical mapping operations. Micro air vehicles (MAVs) could be used to transport items between places, inspect structures for preventative maintenance, and enter hazardous areas to carry out tasks.

The fundamental difference between fixed and flapping wing lift generation is based on the aerodynamic phenomena harnessed by them. Fixed wings use steady mechanisms to achieve lift whereas flapping wings use unsteady mechanisms such as wake capture, leading edge vortices, and circulation effects [8, 6, 19] to produce lift. It could be argued [15] that the unsteady aerodynamics harnessed by flapping wings leads to energy being wasted in generating vortices in the wake of the wing. However, studies [13] have shown that the scaled propulsive efficiency of flapping wings are higher than fixed wing counterparts. The ability of flapping wings to achieve reduced power consumption at low cruising speeds [13] results in better maneuverability in confined spaces. Hovering insects often have a symmetric, periodic back and forth wing motion [27] which could be replicated by resonant mechanisms [3] to achieve the required motion while having lower power consumption. Thus, although rotary wing MAVs such as quadcopters have become ubiquitous in recent times, there is significant merit to studying flapping wing flight.

Much work has been done to study and model [11, 21] the unsteady aerodynamic processes that govern flapping wing lift production. The interaction between these mechanisms and their individual timings with respect to each other have a significant impact on the overall lift generation [6]. Most unsteady models, although accurate in predicting the lift generation, were heavily dependent on empirical parameters or incorporated assumptions such as a rigid wing [16] which does not exhibit passive pitching behavior. The quasi-steady model developed by Wang et al [22] aims to overcome these limitations. This model predicts the aerodynamic forces and torques acting on the wing resulting from the translational, rotational motion of the wing along with coupling and mass effects.

There have been a number of forays [5, 29, 28] into developing flapping wing micro-air vehicles (FWMAVs) but with a larger focus on the overall system and not so frequently the nuances of wing design. For instance, Wood et al [29] use a simple vein like design to mimic the stiffness distribution of insect wings. Similarly, the study by Whitney et al [28] uses a geometrical function to describe the spanwise area distribution (or shape) of the wing based off existing insect wings. Studies conducted by Wang et al [24] approximate the wing geometry into a simplified 1D structure connected by a series of springs which represent the structural stiffness and decouple the root stiffness of the wing to facilitate easier design. Although the same study optimizes several aspects of the wing to maximum lift production, the resulting wing design is a list of wing characteristics that need to be individually produced and assembled. With currently existing rapid prototyping technology, it is possible to incorporate such optimized favourable characteristics into a continuous structure which can be easily 3D printed. There is, therefore, a need to summarize these lift-enhancing parameters and further iterate to achieve better wing designs.

2. Flapping Wing Lift Influencers

Recent trends indicate that there is an interest in miniaturization of robots which means that for the FWMAV, all the individual parts, including the wings will be smaller. When designing a FWMAV with a payload in the gram scale, it is very important to make sure that the individual components are optimized to minimize their weight. Hence, a good wing needs to have minimum weight while still providing high lift. We shall call this the *effective* lift production of the wing. In order to design a wing with high effective lift, we need to look at the aspects of wing geometry and kinematics that influence lift production.

2.1. Wing Kinematics

There have been many studies [26] that have analysed the effect of altering wing kinematics such as flapping frequency, angle of attack at wing tip, timing of wing pitching and stroke reversal, and other factors on the wing lift produc-

ORCID(s):

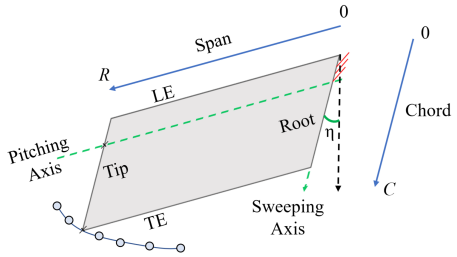

Figure 1: Some of the basic terminology used to describe wing geometry is shown here. LE and TE correspond to the wing's Leading Edge and Trailing Edge respectively. The wing executes a sweeping motion about an axis passing through the wing root, while simultaneously pitching about an axis parallel (in this case) to the LE and TE. This pitching motion causes the wing to attain an angle of attack, η, as shown. The spanwise and chordwise directions are frequently used to describe various characteristics of the wing, such as area and mass distributions.

tion. For instance, the angle of attack is known to be approximately around 35 degrees at 70% of the wingspan [14] for hovering insects. The influence of flapping frequency has also been studied by Wang [25] and the reference flapping frequency for hawkmoths is around 25 Hz [24].

2.2. Pitching Behaviour

During the stroke reversal phase of wing motion, the wing pitches so that the relative positions of the leading and trailing edge of the wing are swapped. This pitching motion is not always actively controlled in insects. Further, an active wing pitch system would add weight [16] in an FWMAV. Hence, it would be preferable to utilize a passive pitching system capable of attaining the required angle of attack at the tip. The drawback of this approach is that passively pitching wings often experiences inertial loads of large magnitude. Experiments conducted by Sane et al [18] show that pitching axis orientation plays a vital role in determining the aerodynamic forces generated. Using their quasi-steady aerodynamic model, Wang et al [24] optimized the pitching axis location thereby achieving reduced power consumption. The resulting optimized designs are shown in Fig 2.

2.3. Area Dsitribution

The influence of wing geometry on mean lift was studied by Ansari et al [1]. Various characteristics such as wing aspect ratio, length, and area were changed for different shapes of the wing planform and their effect on the mean lift generated was studied. It was observed that increasing the above parameters resulted in an increase in wing lift however, the lift-to-drag ratio did not exhibit the same behavior indicating that there could be optimal solutions to be found. Further, the study seems to indicate that there are fundamental differences in the magnitude of lift force generated depending on the shape of the wing planform itself necessitating more research on the spanwise area distribution of the wing.

The wing cross-section, described by the chordwise area distribution, is more important for wings that pitch passively [24] as compared to wings with prescribed kinematics. The impact of this characteristic on lift generation is not yet fully understood.

2.4. Mass Distribution

Similar to the area distribution of the wing, the mass distribution of the wing also has an influence on its aerodynamic performance. Although the spanwise and chordwise mass distribution of many insect wings have been studied [17, 7] and characterized, their impact on lift generation characteristics is not yet fully understood. A little more intuitive to understand is the influence of the chordwise mass distribution of the wing. When the wing undergoes pitching and sweeping, the mass distribution of the wing has a direct correlation with the inertial force experienced by it.

The mass distribution of the wing in the spanwise and chordwise direction relates to the structural stiffness of the wing. Having a wing design that is stiff to inertial and aerodynamic loads while at the same time allows for passive rotations about the pitching axis is, therefore, a design challenge which needs further research.

3. Evaluating a given design

As discussed in previous sections, there are multiple wing parameters that need to be considered when evaluating a given wing design. Although there exist aerodynamic models that predict mean lift generated, these are mostly not applicable for generic wing shapes and wing mass distributions. From an engineering design perspective, it is important to set up a simple framework to computationally evaluate a given wing design under specific load cases and contrast its performance with other designs.

3.1. Modelling of a Wing

Considering a simple rectangular wing geometry as shown in Fig 3, it can be seen that the finite element modelling challenge arises from the ratio of the wing thickness to the wing chord length. In reality, insect wings do not have a uniform thickness, they are made of multiple layers stacked in patterns over each other with venations that run through the planform, providing additional stiffness [4]. Some of the most slender portions of the wing could be as low as 50 microns thick. Compared with the span or chord length of the wing, it can easily be seen that these are extremely slender structures.

For thin plates, there are three major reaction forces that are present under loading conditions, namely - membrane, bending, and couple. Plates symmetric about the mid-plane do not have any couple stresses and therefore, only the former two need to be considered. As the ratio of plate thickness to chord length gets lower, the membrane action kicks in and starts dominating. A wing that is simultaneously translating and rotating through a fluid medium experiences forces that are perpendicular to the surface of the wing as shown in the simple case in Fig 4. This indicates that, for the boundary conditions shown, the forces generated act out-of-plane

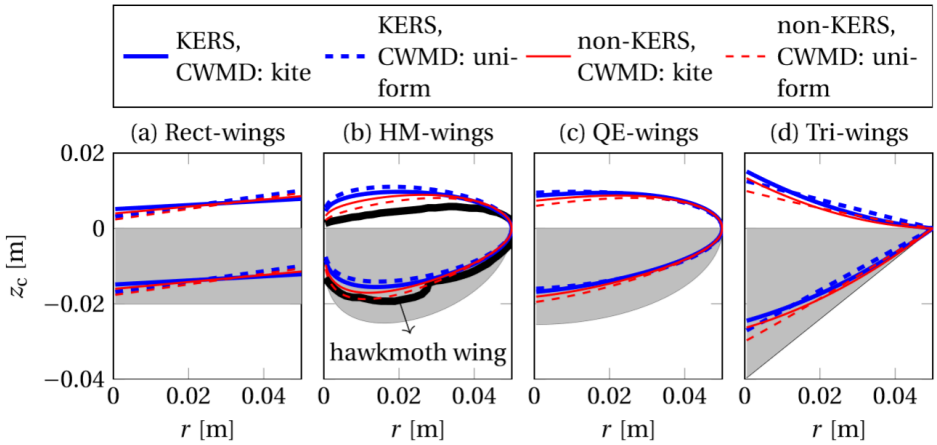

Figure 2: The study conducted by Wang et al [24] aims to optimize the pitching axis location of various wing shapes. Here, KERS refers to a Kinetic Energy Recovery System with which the kinetic energy of the wing during deceleration phase can be used to compensate for the energy consumed by drag. CWMD refers to the Chordwise Mass Distribution of the wing.

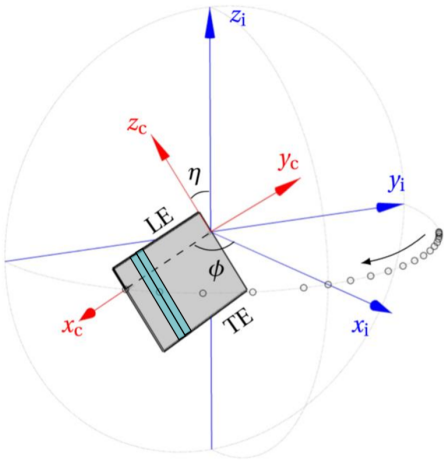

Figure 3: The figure shows the basic geometry of a rectangular wing planform. Translational component of the flapping motion can be described as a rotation about the local z_c axis. The pitching axis, in this case, is aligned with the local x_c axis. A simplified approach for modelling, carried out by Wang et al [24] was to divide the wing into rigid, chordwise strips as shown. This allowed for modelling of the twisting of the wing in an easier manner.

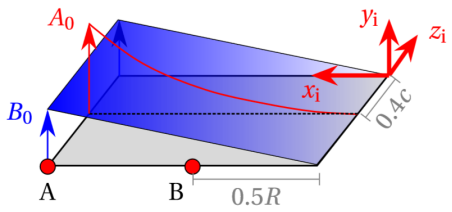

Figure 4: A rectangular wing under loading conditions derived by Wang et al [24]. The inertial load, represented in blue, is a surface load acting on the wing due to it's rotation about the local z_c axis. The aerodynamic load, represented by the red curve is modelled as a parabolic line load. On an actual wing, the aerodynamic load is a pressure load that always acts perpendicular to the surface of the wing planform. This approximation is valid for Wang's model as each chordwise strip is considered to be rigid.

with respect to the wing planform. Therefore, it can be expected that a larger portion of the deformation will be due to rotation rather than stretching. The magnitude of the rotation at the wing tip, which is around 45 degrees, falls in the regime of finite rotations [10].

The above-mentioned aspects of the wing geometry and deformation imply the need for nuanced finite element modelling of the problem. The slenderness of the wing geometry allows for the use of computationally cheaper shell elements. However, these elements need to account for membrane deformation and should also be able to handle finite rotations. Despite accounting for all of these conditions, the non-linear nature of the problem stands to cause further complications under specific load cases. The element developed by Van Keulen et al [20] is very apt for this case as it incorporates additional terms to reflect membrane contribution and has a consistent finite rotation formulation.

3.2. Load Cases

The flapping wing experiences an aerodynamic pressure load and an inertial load on its surface. The study by Wang et al [23] divides the wing into a number of rigid chordwise strips along the span of the wing. This allows for twisting of the wing via relative rotation of one strip with respect to another. The aerodynamic force, which acts on each chordwise strip can be approximated as a point force acting at a centre of pressure on the chord. This allowed the researchers to simplify the aerodynamic surface load as a line load for

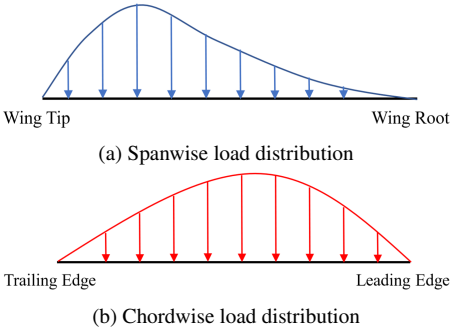

(a) Spanwise load distribution

(b) Chordwise load distribution

Figure 5: The pressure load profile in the spanwise and chordwise directions are shown in this figure. Although the spanwise distribution somewhat maintains the same profile through the flapping stroke, the chordwise distribution undergoes changes. However, this shape is considered to be a sufficient approximation of the mid-stroke load distribution. Further refinements in load distribution patterns are necessary for more accurate results.

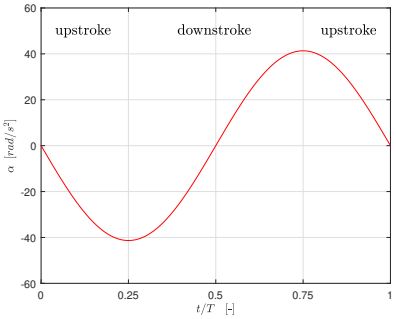

Figure 6: A flapping wing that executes a harmonic motion with the time-normalized instantaneous angular acceleration varying throughout the stroke as shown. Points of interest are the start of the downstroke and upstroke at $\frac{t}{T} = 0.25$ and $\frac{t}{T} = 0.75$ respectively.

the simple rectangular wing as shown in Fig 4. When considering a fully flexible wing, this simplification needs to be reversed as each chordwise strip is no longer rigid.

3.2.1. Aerodynamic Load

A straightforward way of going back to the surface load is by approximating the aerodynamic load distribution along the chord using a cubic surface fit. This allows for reasonable flexibility in choosing shape functions for finite element modelling and also allows for a balanced computation time as a lower number of quadrature points can sufficiently evaluate the integral. Although this is an approximation of the true load profile, it is considered sufficient for the purpose of this study. The aerodynamic load varies in the chordwise and spanwise directions as shown in Fig 5.

The centre of pressure of the aerodynamic load in the chordwise direction is known to range from 1/4 to mid-chord [12] and the approximate spanwise distribution of the aerodynamic load is also known [2]. Using this information, a set of equations were used to develop a cubic surface given the locations of the centres of pressure in chordwise and spanwise direction, the span length, and the chord length of the wing. This is documented in detail in Appendix A. A cubic pressure load distribution was obtained as shown in Fig 8 for a rectangular wing with span = 5 cm and chord = 2 cm. It must be noted that the dependence of the aerodynamic load on the shape of the wing planform was not developed. An approximation of the shape-dependent nature was achieved by shifting the cubic load surface to reflect the changing centre of pressure when the shape of the wing is altered. However, rigorous implementation of the relation between wing shape and aerodynamic load distribution was not deemed necessary for the purpose of this study as the inertial loads (for a passively pitching wing) are known to be dominant for most phases of the stroke. Hence, wing deformation characteristics under such inertial loads were considered in detail for this study.

3.2.2. Inertial Load

The inertial load consists mainly of the tangential force contribution due to the rotation of the wing about the wing root, (i.e., the sweeping motion). This is simply calculated for each element as $F^i = m^i r^i \alpha$ where m^i is the mass of the i-th element, r^i is the radial distance of the element from the axis of rotation, and α is the instantaneous angular acceleration of the wing, which varies throughout the stroke as shown in Fig 6. The radial distance of the element is simply the x_c local coordinate of the wing in the undeformed configuration as can be seen from Fig 3.

3.2.3. Flapping Stroke Phases

The model developed by Wang et al [22] was used to predict the lift force generated for a harmonic sweeping motion of a wing. The described motion results in a time-normalized angular acceleration which varies throughout the stroke as shown in Fig 6 and the lift and drag forces for a twistable wing varying as shown in Fig 7.

From the above-mentioned figures, the variation of aerodynamic and inertial forces during the upstroke and downstroke can be clearly seen. The mid- upstroke and mid- downstroke phases, indicated by $\frac{t}{T} = 0$ and $\frac{t}{T} = 0.5$ respectively, are phases of maximum lift generation. Whereas, from Fig 6 it can be seen that during these phases, the inertial load is zero. Another region of interest is the end of the upstroke phase and downstroke phase at $\frac{t}{T} = 0.25$ and $\frac{t}{T} = 0.75$. These regions have almost no aerodynamic force acting on the wing but the inertial load is at a maximum. This may not be very interesting for wings with a uniform thickness distribution, as this would result in a very uniform load profile acting on the surface of the wing planform. For wings with a varying thickness distribution, however, areas of concentrated mass would experience a larger inertial load which may lead to an interesting deformation profile of the wing.

The stroke phases which mark the transition either from

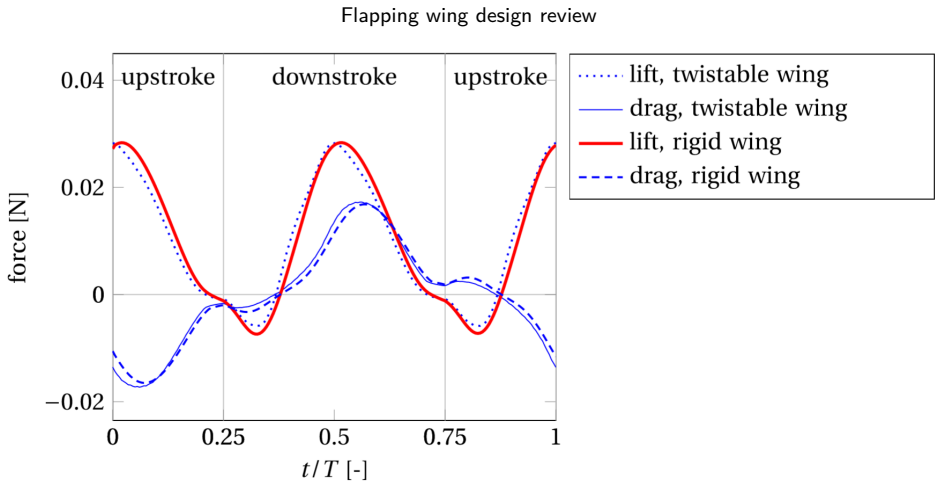

Figure 7: Wang et al [22] developed a quasi-steady aerodynamic model and used it to predict the lift and drag forces generated on a wing executing a harmonic sweeping motion. The horizontal axis indicates normalized time.

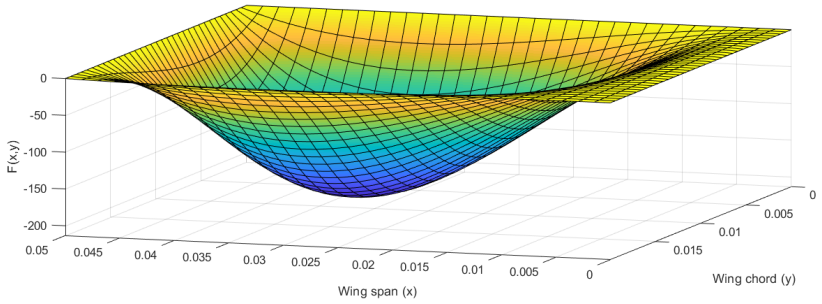

Figure 8: A cubic load surface distribution was obtained for the aerodynamic load for a rectangular wing with span $(r) = 5$ cm and chord $(c) = 2$ cm. MATLAB's *fsolve* function was used to solve a set of nonlinear equations and obtain the surface equation. A detailed description of the derivation is available in Appendix A.

up- to downstroke or vice versa, corresponding to $\frac{t}{T} = 0.125$ and $\frac{t}{T} = 0.625$ also need to be studied. These are regions where both aerodynamic and inertial loads are acting on the wing. During these phases, when the wing experiences forces acting in multiple directions, it needs to be stiff in bending while also maintaining the required angle of attack. Hence, there are 3 phases of the stroke that need to be analysed - the mid-stroke, the transition phase, and the end of the stroke. For a harmonic sweeping motion, it is sufficient to study these phases for either the upstroke or the downstroke due to the symmetric nature of the wing motion. Note that for mid-stroke phase, if there are no inertial loads acting on the wing at that instant, the wing cannot be expected to deform and passively pitch unless the aerodynamic forces are of high enough magnitude and the centre of pressure is situated such that it generates a significant torque about the pitching axis.

3.3. Evaluation Parameters

Considering the difficulty of conducting full transient analyses for a highly nonlinear structure such as the flapping wing, it makes a lot of sense from an engineering design perspective to consider only certain important phases of the wing stroke. The stroke phases mentioned prior can be used as individual quasi-static load cases to study the deformation of the wing. When comparing two given wing designs loaded under each of these load cases, it is necessary to look at certain parameters as listed.

(1) **Angle of attack:** Under the applied loads, the wing should deform such that the required angle of attack is achieved. For instance, a wing span of 5 cm would require an angle of attack of 45 degrees at the wing tip under high magnitude inertial loads. In case the triangular shell element used by Van Keulen et al [20] is used, the rotation of the midside nodes at the wing tip can be checked.

(2) **Bending deformation:** The wing should be stiff under the applied loads, meaning that it should not bend significantly in the direction of the normal to the wing planform. This can be checked by looking at the vertical (or out-of-plane) displacement of the nodes at the wing tip. Assuming that the loads applied are continuous, this should theoretically result in a continuous deformation field as well.

(3) **Pitching axis orientation:** The pitching axis should be oriented along the previously described optimal direc-

tion corresponding to the shape of the wing planform. The displacement corresponding to nodes on the required pitching axis should be minimal and this would allow those nodes to act as the axis about which the wing pitches.

(4) **Deformation profile:** The deformed configuration of the wing should be continuous, i.e., there are no kinks, wrinkles, or folds formed due to buckling. The slender nature of the wing means that certain nonlinear behaviour could be exhibited by the problem, especially if the solver has not correctly converged. This needs to be checked and it should be made sure that the solution has correctly converged.

4. Summary and Conclusion

This study aims to collate the data from other studies on flapping wing lift generation and come up with a simple way to numerically evaluate the effective lift generation of a given wing geometry using a list of easily comparable parameters. These parameters are picked such that a simple static analysis of the wing design under a given load case gives insight on the performance of the wing. For instance, a wing design that bends more than another given design under identical load cases would be inferior in terms of lift generation. The loads under which these parameters are to be compared are also described in detail and a method of changing from a 1D load description to a 2D description was developed. This kind of simple numerical testing of the wing allows designers to come up with good wing designs without the need of conducting intense fluid-structure interaction studies or full transient analyses on the wing. It is important to note that this serves as a preliminary evaluation of wing design. For a more detailed evaluation of the wing, it is indeed necessary to carry out the above mentioned analyses.

References

[1] Ansari, S.A., Knowles, K., Zbikowski, R., 2008. Insectlike Flapping Wings in the Hover Part II: Effect of Wing Geometry. Journal of Aircraft 45, 1976–1990. URL: http://arc.aiaa.org/doi/10.2514/1.35697, doi:10.2514/1.35697.

[2] Betteridge, D.S., Archer, R.D., 1974. A Study of the Mechanics of Flapping Wings. Aeronautical Quarterly 25, 129–142. URL: https://www.cambridge.org/core/article/study-of-the-mechanics-of-flapping-wings/067B10F56E41199BAD4C8424C9F10077, doi:DOI:10.1017/S0001925900006892.

[3] Bolsman, C.T., 2010. Flapping wing actuation using resonant compliant mechanisms.

[4] Combes, S.A., Daniel, T.L., 2003. Flexural stiffness in insect wings I. Scaling and the influence of wing venation. Journal of Experimental Biology 206, 2979 LP – 2987. URL: http://jeb.biologists.org/content/206/17/2979.abstract, doi:10.1242/jeb.00523.

[5] DeLaurier, J.D., 1994. An ornithopter wing design. Canadian Aeronautics and Space Journal 40, 10–18.

[6] Dickinson, M.H., Lehmann, F., Sane, S.P., 1999. Wing rotation and the aerodynamic basis of flight. Science 284, 1954–1960.

[7] Dudley, R., Ellington, C.P., 1990. Mechanics of Forward Flight in Bumblebees: I. Kinematics and Morphology. Journal of Experimental Biology 148, 19 LP – 52. URL: http://jeb.biologists.org/content/148/1/19.abstract.

[8] Ellington, C.P., van den Berg, C., Willmott, A.P., Thomas, A.L.R., 1996. Leading-edge vortices in insect flight. Nature 384, 626–630. URL: https://doi.org/10.1038/384626a0, doi:10.1038/384626a0.

[9] Floreano, D., Wood, R.J., 2015. Science, technology and the future of small autonomous drones. Nature 521, 460–466. doi:10.1038/nature14542, arXiv:arXiv:1011.1669v3.

[10] Koiter, W.T., Simmonds, J.G., 1973. Foundations of shell theory BT - Theoretical and Applied Mechanics, Springer Berlin Heidelberg, Berlin, Heidelberg. pp. 150–176.

[11] Laurier, J.D., 1993. An aerodynamic model for flapping-wing flight. The Aeronautical Journal 97, 125–130. doi:10.1017/S0001924000026002.

[12] Liang, Z., Qingfeng, H., Xinyan, D., P., S.S., 2010. Aerodynamic effects of flexibility in flapping wings. Journal of The Royal Society Interface 7, 485–497. URL: https://doi.org/10.1098/rsif.2009.0200, doi:10.1098/rsif.2009.0200.

[13] Liu, T., 2008. Comparative Scaling of Flapping- and Fixed-Wing Flyers. AIAA Journal 44, 24–33. doi:10.2514/1.4035.

[14] P., E.C., James, L.M., 1984. The aerodynamics of hovering insect flight. III. Kinematics. Philosophical Transactions of the Royal Society of London. B, Biological Sciences 305, 41–78. URL: https://doi.org/10.1098/rstb.1984.0051, doi:10.1098/rstb.1984.0051.

[15] Pesavento, U., Wang, Z.J., 2009. Flapping wing flight can save aerodynamic power compared to steady flight. Physical Review Letters 103, 1–4. doi:10.1103/PhysRevLett.103.118102.

[16] Platzer, M.F., Jones, K.D., Young, J., S. Lai, J.C., 2008. Flapping Wing Aerodynamics: Progress and Challenges. AIAA Journal 46, 2136–2149. doi:10.2514/1.29263.

[17] Porter, E.C., James, L.M., 1984. The aerodynamics of hovering insect flight. II. Morphological parameters. Philosophical Transactions of the Royal Society of London. B, Biological Sciences 305, 17–40. URL: https://doi.org/10.1098/rstb.1984.0050, doi:10.1098/rstb.1984.0050.

[18] Sane, S.P., Dickinson, M.H., 2002. The aerodynamic effects of wing rotation and a revised quasi-steady model of flapping flight. Journal of Experimental Biology 205, 1087 LP – 1096. URL: http://jeb.biologists.org/content/205/8/1087.abstract.

[19] Usherwood, J.R., Ellington, C.P., 2002. The aerodynamics of revolving wings I. Model hawkmoth wings. Journal of Experimental Biology 205, 1547 LP – 1564. URL: http://jeb.biologists.org/content/205/11/1547.abstract.

[20] Van Keulen, F., Booij, J., 1996. Refined Consistent Formulation of a Curved Triangular Finite Rotation Shell Element. International Journal for Numerical Methods in Engineering 39, 2803–2820. URL: https://doi.org/10.1002/(SICI)1097-0207(19960830)39:16{%}3C2803::AID-NME977{%}3E3.0.COhttp://2-2, doi:10.1002/(SICI)1097-0207(19960830)39:16<2803::AID-NME977>3.0.CO;2-2.

[21] Vest, M., Katz, J., 2013. Unsteady aerodynamic model of flapping wings 34, 1435–1440. doi:10.2514/6.1995-747.

[22] Wang, Q., Goosen, J.F., Van Keulen, F., 2016. A predictive quasi-steady model of aerodynamic loads on flapping wings. Journal of Fluid Mechanics 800, 688–719. doi:10.1017/jfm.2016.413.

[23] Wang, Q., Goosen, J.F.L., van Keulen, F., 2017a. An efficient fluidstructure interaction model for optimizing twistable flapping wings. Journal of Fluids and Structures 73, 82–99. URL: http://www.sciencedirect.com/science/article/pii/S0889974617300932, doi:https://doi.org/10.1016/j.jfluidstructs.2017.06.006.

[24] Wang, Q., Goosen, J.F.L., van Keulen, F., 2017b. Optimal pitching axis location of flapping wings for efficient hovering flight. Bioinspiration & Biomimetics 12, 56001. URL: http://dx.doi.org/10.1088/1748-3190/aa7795, doi:10.1088/1748-3190/aa7795.

[25] Wang, Z.J., 2000. Vortex shedding and frequency selection in flapping flight. Journal of Fluid Mechanics 410, 323–341. URL: https://www.cambridge.org/core/article/vortex-shedding-and-frequency-selection-in-flapping-flight/1C2EC600C1DF0CBBFBD3928CAFECAC1E, doi:DOI:10.1017/S0022112099008071.

[26] Wang, Z.J., 2004. Dissecting Insect Flight. Annual Review

of Fluid Mechanics 37, 183–210. URL: https://doi.org/10.1146/annurev.fluid.36.050802.121940, doi:10.1146/annurev.fluid.36.050802.121940.

[27] Weis-fogh, Torkel, B., 1973. Fitness in Hovering Animals , Including Novel Mechanisms for Lift Production. Journal of Experimental Biology 59, 169–230. URL: http://jeb.biologists.org/content/59/1/169.short.

[28] Whitney, J.P., Wood, R.J., 2012. Conceptual design of flapping-wing micro air vehicles doi:10.1088/1748-3182/7/3/036001.

[29] Wood, R.J., 2007. Design , fabrication , and analysis of a 3DOF , 3cm flapping-wing MAV , 1576–1581.

A. Appendix I - Cubic Load Surface

This section covers the development of a cubic surface for a recntagular wing planform. For the purpose of this section, the spanwise direction will be denoted by x and the chordwise direction by y. It is chosen to develop the equation of the cubic surface $z = f(x, y)$ as

$$z = f(x, y) = f(x)f(y)$$

The x and y direction equations are cubic in the form

$$g_1(x) = a_1x^3 + b_1x^2 + c_1x + d_1$$

$$g_2(y) = a_2y^3 + b_2y^2 + c_2y + d_2$$

The cubic surface's zero values need to be described. Say the wing's span length is denoted by r and its chord length by c. The function value at $x = 0 \to r, y = 0 \to c$ should be zero. This condition gives us the following equations.

For $x = 0$, we have

$$f(x = 0, y) = g_1(x = 0)g_2(y) = 0 \quad \forall \ y \in \mathrm{R}$$

$$\because \ g_2(y) \neq 0, \ \text{ we have } \ g_1(x = 0) = 0$$

This gives us the equation

$$g_1(x = 0) = d_1 = 0 \tag{1}$$

The equations at $x = r$ are

$$f(x = r, y) = g_1(x = r)g_2(y) = 0 \quad \forall \ y \in \mathrm{R}$$

$$\because \ g_2(y) \neq 0, \ \text{ we have } \ g_1(x = r) = 0$$

Leading to the equation

$$g_1(x = r) = a_1r^3 + b_1r^2 + c_1r = 0 \quad (\because \ d_1 = 0) \tag{2}$$

Similarly, the equations for $g_2(y)$ are derived. First, once more, for $y = 0$, we have

$$f(x, y = 0) = g_1(x)g_2(y = 0) = 0 \quad \forall \ x \in \mathrm{R}$$

$$\because \ g_1(x) \neq 0, \ \text{ we have } \ g_2(y = 0) = 0$$

This leads to the equation

$$g_2(y = 0) = d_2 = 0 \tag{3}$$

Then, for $y = c$, the equations come out to be

$$f(x, y = c) = g_1(x)g_2(y = c) = 0 \quad \forall \ x \in \mathrm{R}$$

$$\because \ g_1(x) \neq 0, \ \text{ we have } \ g_2(y = c) = 0$$

Giving us

$$g_2(y = 0) = a_2c^3 + b_2c^2 + c_2c = 0 \quad (\because \ d_2 = 0) \tag{4}$$

Next, the peaks of the surface can be controlled by using one of two approaches. One approach is to constrain the slope of the curve. Another approach would be to constrain the centroid of the curve. For this study, it was chosen to use the former. If the peak of the surface in the spanwise direction occurs at a point $x = x_*$, the following equations hold true for all values of y.

$$\left.\frac{\partial f(x, y)}{\partial x}\right|_{x=x_*} = g_2(y)\left.\frac{\partial g_1(x)}{\partial x}\right|_{x=x_*} = 0$$

$$\because \ g_2(y) \neq 0, \ \text{ we have } \ \left.\frac{\partial g_1(x)}{\partial x}\right|_{x=x_*} = 0$$

$$\left.\frac{\partial g_1(x)}{\partial x}\right|_{x=x_*} = 3a_1x_*^2 + 2b_1x_* + c_1 = 0 \tag{5}$$

Similarly, if the peak of the surface in the chordwise direction is known to occur at $y = y_*$ for all values of x, we have

$$\left.\frac{\partial f(x, y)}{\partial y}\right|_{y=y_*} = g_1(x)\left.\frac{\partial g_2(y)}{\partial y}\right|_{y=y_*} = 0$$

$$\because \ g_1(x) \neq 0, \ \text{ we have } \ \left.\frac{\partial g_2(y)}{\partial y}\right|_{y=y_*} = 0$$

$$\left.\frac{\partial g_2(y)}{\partial y}\right|_{y=y_*} = 3a_2y_*^2 + 2b_2y_* + c_2 = 0 \tag{6}$$

The last set of equations come from setting appropriate integral values for the surface. The surface integral can be chosen to have a certain value depending on the net force, P desired on the wing planform as shown below.

$$\int_0^c \int_0^r f(x, y)dxdy = \int_0^c \int_0^r g_1(x)g_2(y)dxdy = P$$

$$\left(\frac{a_1r^4}{4} + \frac{b_1r^3}{3} + \frac{c_1r^2}{2} + d_1r\right)\left(\frac{a_2c^4}{4} + \frac{b_2c^3}{3} + \frac{c_2c^2}{2} + d_2c\right) = P \tag{7}$$

Similarly, a constraint can be imposed on the integral on either the spanwise or chordwise direction. This can be thought of as a tuning parameter which controls the relative heights of the peaks in each direction. In this case, the spanwise approach is used and the integral is constrained to have a value I at the point $y = y_*$.

$$\int_0^r f(x, y)dx = f(y)\int_0^r g_1(x)dx = I$$

$$\left(\frac{a_1 r^4}{4} + \frac{b_1 r^3}{3} + \frac{c_1 r^2}{2} + d_1 r\right)\left(a_2 y_*^3 + b_2 y_*^2 + c_2 y_*\right) = I \tag{8}$$

Therefore, in order to find the value of 8 unknown coefficients, we have obtained 8 equations. These equations can be solved numerically using MATLAB function `fsolve` using the Levenberg-Marquardt algorithm in a straightforward manner.

Chapter 4

Technical Paper

This chapter presents a technical paper which was written as part of the thesis project. The paper aims to optimize wing geometry to achieve high effective lift using the thickness distribution as the design variable. A sensitivity implementation for such problems is presented and implementation aspects are described in detail in the appendix. Finally, results for a rectangular wing shape and a hawkmoth wing shape under various loading conditions are shown.

Optimization of Thickness Distribution in Flapping Wings

A. Narayanan, Dr. ir. J.F.L. Goosen and Prof. dr. ir. A. van Keulen

ARTICLE INFO

Keywords:
flapping wing
design
optimization
thickness sensitivity

ABSTRACT

This study aims to use the qualitative parameters established in the preceding paper to conduct an optimization study which uses element thickness as the design variable for a flapping wing with fixed planform under various loading cases. The implementation of sensitivity is discussed for symmetric slender structures which need to include membrane terms. The load cases are described for different phases of the stroke cycle and their implementation is also discussed. The obtained wing geometries under each of the load cases are studied and compared. The optimized rectangular wing planform achieved an angle of attack of 43.15 degrees at the wing tip under high magnitude inertial loads whereas the hawkmoth wing shape achieved an angle of 39.81 degrees at 60% of the wing span under the same load. Finally, general thickness distribution patterns obtained by the optimizer are highlighted and discussed.

1. Introduction

Research on insect robots has become more prevalent over the last several years due to their extensive applications in various industries such as agriculture, defense, surveillance, mapping, and rescue operations [3]. The small size of these drones allows them to access areas otherwise inaccessible and also gives them advantages in terms of maneuvrability. It is also possible that in the future, swarms of such insect robots would carry out various tasks in synchronization, leading to reduced manual labour. This study is focused on the category of micro air vehicles (MAVs) which use flapping wings to generate lift, similar to various flying insects such as the hawkmoth, and the dragonfly.

The unsteady aerodynamics generated by flapping wings results in their ability to hover efficiently and consume less power at their lower cruising speeds when compared to proportionally scaled fixed wing aircraft [4]. The unsteady aerodynamics that govern the lift generation behind flapping flight have been studied in detail [2, 1, 6]. Phenomena such as the leading edge vortex, rotational circulation, and wake capture are complex and computationally demanding to simulate. When comparing two given wing designs, it is more efficient to rate each wing based on a few simple parameters that can be measured computationally relatively easily. The first part of this study covers this in further detail and lists parameters such as the bending stiffness of the wing, and the angle of attack at the tip which can be checked under specific load cases. These parameters can also be used as constraints for an optimization study to come up with different optimal designs for each load case considered, which is the aim of this study.

For topology optimization, a pseudo-density based approach is generally employed where the stiffness matrix is pre-multiplied by a density term in the constitutive equations. However, this affects the way sensitivities are calculated. In case of slender structures such as the wing, it is important to consider the membrane-related terms. Since the flapping wing is considered to be symmetric about the mid-plane, the coupling terms that relate membrane and bending action can be neglected. This is covered in more detail in Sec 2.1.

ORCID(s):

2. Optimization Problem

As discussed in the first part of this study, the parameters that can be used to compare given wing designs are listed and these can further be used to constrain the optimizer. A well-defined problem needs well-described loads, constraints and a sensible objective function and all of these are discussed in further detail below.

2.1. Sensitivity Implementation

The influence of membrane action gets more significant as the thickness to chord length ratio gets reduced and hence, a pseudo-density SIMP formulation is not sufficient for this case. The density based topology optimization approach is shown in Eq 1, where it can be seen that the stiffness tensor for each element E^0_{ijkl} is premultiplied with a penalized pseudo-density term $\rho(x)^p$. The effective stiffness of each element is therefore dependent on this pseudo-density term, which acts as the design variable. The penalization factor is used to tune how aggressively the optimizer allocates material to each element. A higher penalization exponent discourages any so-called grey designs and forces the optimizer to come up with solid-void designs that can be manufactured.

$$\begin{aligned} E_{ijkl}(x) &= \rho(x)^p E^0_{ijkl} \quad , p > 1 \\ \int_\Omega \rho(x) d\Omega \leq V \quad &\text{s.t.} \quad 0 \leq \rho(x) \leq 1, \quad x \in \Omega \end{aligned} \tag{1}$$

The pseudo-density approach cannot be applied for thickness sizing of slender structures such as the wing, however, due to the membrane and bending stiffnesses changing with the thickness of the element. This means that the original stiffness tensor for each element, given before by E^0_{ijkl}, will change as the thickness of the element is modified. For this study, an initial thickness t^0 for the whole plate is set and the element thickness is calculated as $t_e = s_e t^0$. Using this

formulation, the design variable is not the element thickness itself but the dimensionless scaling factor for each element.

A nonlinear finite element analysis works by solving the equilibrium equation between the internal force and the external force as shown below, where λ is the load multiplication factor used in the Newton-Raphson iteration scheme.

$$\mathbf{f}^{\text{int}} = \lambda \mathbf{f}^{\text{ext}}$$

The adjoint compliance method is used to calculate the sensitivities for a response function say $r(s; u(s))$ where s denotes the design variable and $u(s)$ denotes the displacement field which is a function of the design variable. The augmented response function used in th adjoint formulation is given below.

$$r^* = r(s; u(s)) + \mu \left[\mathbf{f}^{\text{int}}(s; u(s)) - \lambda \mathbf{f}^{\text{ext}}(s; u(s))\right]$$

As can be seen from the above, complications arise for the flapping wing case as the external load is dependent on the design variable and also the displacement of the wing as described in the first part of this paper. The adjoint term μ needs to be calculated such that the coefficients of $\frac{du}{ds}$ are discarded. The term from the displacement-dependent external load is ignored for the purpose of this research as that is a topic that requires further research and also the implicit dependence of displacement on the design variable indicates that the optimizer will converge, although slowly.

$$\frac{\partial r^*}{\partial s} = \frac{\partial r}{\partial s} + \left[\frac{\partial r}{\partial u} + \mu \left(\frac{\partial \mathbf{f}^{\text{int}}}{\partial u} - \lambda \frac{\partial \mathbf{f}^{\text{ext}}}{\partial u}\right)\right] \frac{du}{ds} + \mu \left[\frac{\partial \mathbf{f}^{\text{int}}}{\partial s} - \lambda \frac{\partial \mathbf{f}^{\text{ext}}}{\partial s}\right]$$

If the adjoint parameter is calculated appropriately, we are left with the following equation where $\frac{\partial \mathbf{f}^{\text{ext}}}{\partial s}$ can be calculated in a straightforward manner from $F_{inertial} = m.r.\alpha$ for an object rotating about a given axis.

$$\frac{\partial r^*}{\partial s} = \frac{\partial r}{\partial s} + \mu \left[\frac{\partial \mathbf{f}^{\text{int}}}{\partial s} - \lambda \frac{\partial \mathbf{f}^{\text{ext}}}{\partial s}\right]$$

The internal force is related to the generalized stresses by

$$\mathbf{f}^{\text{int}} = \mathbf{D}^{\text{T}} \sigma$$

where σ are the generalized stresses. Essentially, in order to calculate the sensitivity of the internal force with respect to the design variable, it is necessary to calculate the sensitivity of the generalized stresses. The relation between the stress resultants and couples, and the stretching deformation and curvature changes for a plate is given in Eq 2.

$$\begin{bmatrix} N_{xx} \\ N_{yy} \\ N_{xy} \\ \dots \\ M_{xx} \\ M_{yy} \\ M_{xy} \end{bmatrix} = \begin{bmatrix} \mathbf{A} & \vdots & \mathbf{B} \\ \dots & \dots & \dots \\ \mathbf{B} & \vdots & \mathbf{D} \end{bmatrix} \begin{bmatrix} \gamma_{xx} \\ \gamma_{yy} \\ \gamma_{xy} \\ \dots \\ \kappa_{xx} \\ \kappa_{yy} \\ \kappa_{xy} \end{bmatrix} \tag{2}$$

The stress measures are related to the deformations through the **A-B-D** matrix, which is dependent on the design variable. Here, the components of the **A-B-D** matrix, which relates the tangential stress couples and resultants to the stretching and curvature changes, are given in Eq 3. $\mathbf{Q}(z)$ is a matrix that describes material behavior at a distance z from the mid-plane. In case of a plate that is symmetric about the mid-plane, the coupling **B** matrix is zero which simplifies the equations considerably. Further, the difference in scaling of the **A** and **D** matrices must be noted. It can be seen that the **A** matrix is linearly proportional to the plate (or element) thickness, while the **D** matrix has a cubic relation with the plate element thickness. Due to this difference in proportionality, sensitivities need to be calculated correctly. It should be noted that if this were a pure bending or pure stretching problem, one could still opt for the pseudo-density.

$$\begin{aligned} \mathbf{A} &= \int_{-\frac{h}{2}}^{+\frac{h}{2}} \mathbf{Q}(z) dz \\ \mathbf{B} &= \int_{-\frac{h}{2}}^{+\frac{h}{2}} z\mathbf{Q}(z) dz \\ \mathbf{D} &= \int_{-\frac{h}{2}}^{+\frac{h}{2}} z^2\mathbf{Q}(z) dz \end{aligned} \tag{3}$$

One approach to implementing the sensitivities in this case would be to use the perturbation method. This can be done by perturbing the thickness of the element with an appropriate step size and thereby calculating the sensitivities of the stress resultants and couples with respect to the element thickness. However, this would be computationally expensive as the sensitivities would need to be recalculated after every iteration for every element.

2.1.1. General Asymmetric Plate Approach

A general approach has been developed for the plate thickness sizing problem by decoupling the **A-B-D** matrix into the **A-D** matrix and the **B** matrix as shown in Eq 4.

$$\begin{bmatrix} \mathbf{A} & \vdots & \mathbf{B} \\ \dots & \dots & \dots \\ \mathbf{B} & \vdots & \mathbf{D} \end{bmatrix} = \begin{bmatrix} \mathbf{A} & \vdots & \mathbf{0} \\ \dots & \dots & \dots \\ \mathbf{0} & \vdots & \mathbf{D} \end{bmatrix} + \begin{bmatrix} \mathbf{0} & \vdots & \mathbf{B} \\ \dots & \dots & \dots \\ \mathbf{B} & \vdots & \mathbf{0} \end{bmatrix} \tag{4}$$

If the **A-B-D** matrix is multiplied by a scalar t_e^p, it acts as a penalization factor which encourages the optimizer to opt for high-low thicknesses instead of a smooth distribution. For the **A-D** matrix, a new **F** matrix (Eq 5) is developed which can be multiplied with it to generate the required sensitivities. Here, **I** is a 3 X 3 identity matrix and p denotes the thickness penalization exponent, a scalar quantity.

$$\mathbf{F} = \begin{bmatrix} \mathbf{I} * (p+1) & \vdots & \mathbf{0} \\ \cdots & \cdots & \cdots \\ \mathbf{0} & \vdots & \mathbf{I} * (p+3) \end{bmatrix} \tag{5}$$

The **B** matrix, on the other hand, needs to be multiplied by a scalar factor of $(p+2)$ to obtain the required sensitivities. The final, derivative of the **A-B-D** matrix with respect to the design variable is given by the relation in Eq 6.

$$\frac{d\textbf{A-B-D}}{ds_e} = (\textbf{A-D} * \mathbf{F}) + (\mathbf{B} * (p+2)) \tag{6}$$

2.1.2. Symmetric Plate Approach

An even simpler approach could be implemented for plates which are symmetric about the mid-plane. Instead of modifying the **A-B-D** matrix, the stress vector is directly modified by multiplying the tangential stress resultants by a factor of $(p+1)$ and the stress couples by a factor $(p+3)$ as shown in Eq 7.

$$\frac{d\sigma}{ds_e} = \begin{bmatrix} N_{xx}(p+1) \\ N_{yy}(p+1) \\ N_{xy}(p+1) \\ \cdots \\ M_{xx}(p+3) \\ M_{yy}(p+3) \\ M_{xy}(p+3) \end{bmatrix} \tag{7}$$

The symmetric plate approach was implemented for the current study due to its simplicity and validated using the finite difference method. The data from this validation study is tabulated in Appendix A.

2.2. Load Cases

The wing experiences forces acting on its surface which change direction and magnitude throughout the flapping stroke. The aerodynamic force is a pressure load which acts perpendicular to the surface of the wing planform. The inertial load, on the other hand, is a surface load which acts along the line of motion of the wing. The direction in which it acts is determined by the instantaneous angular acceleration of the wing. It is, therefore, not a follower load as opposed to the aerodynamic load. For the optimization study, a harmonic sweeping motion of the wing was considered, with the angular acceleration of the wing varying throughout the stroke. Due to the symmetric nature of the motion, the wing deformation behaviour was studied only during the upstroke. Although there are certain portions of the downstroke where the loads are acting in different directions, the magnitude of the aerodynamic load is much lower than the inertial forces that a passively pitching wing experiences and hence, the above restriction is deemed appropriate.

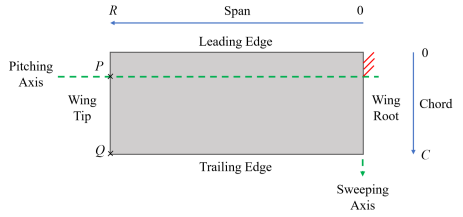

Figure 1: Basic wing nomenclature is shown in this figure. The rectangular wing performs a sweeping motion about an axis passing through the wing root, and pitches about the pitching axis. The pitching motion causes it to have an angle of attack.

Based on a qualitative approach, certain portions of the flapping stroke are considered and the corresponding net aerodynamic force and time-normalized angular acceleration are recorded in Table 1. A cubic pressure load distribution was developed in the first part of this study as an approximate representation of the aerodynamic pressure acting on the wing. Existing shell element research code was used to conduct the FEA, however certain updates were made to accommodate non-uniform pressure distributions and these changes have been documented in Appendix B.

2.3. Problem Formulation

Under applied loads, the wing needs to be stiff in bending while still being able to passively pitch and obtain the required angle of attack at the wing tip. Formulating this as a compliance minimization problem could prevent the optimizer from allowing the wing to be compliant enough to twist and achieve the angle of attack. Hence, the optimization problem is simply defined as a displacement maximization problem, where a point on the wing's trailing edge close to the wing tip is chosen to have a certain displacement that allows for an angle of attack at the wing tip under applied loading conditions. For instance, in Fig 1, the point of intersection of the wing trailing edge and the wing tip, denoted by point Q, is chosen to have high vertical displacement. Simultaneously, the point of intersection of the pitching axis and the wing tip, denoted by point P, is constrained to have very low displacement. This is mathematically formulated below. Note that u_z denotes the magnitude of the vertical out-of-plane displacement of the point.

$$\begin{aligned} &\min \ (-u_z^Q) \\ &\text{s.t.} \quad u_z^Q \leq u_{\max}^Q, \\ &u_{\min}^P \leq u_z^P \leq u_{\max}^P \end{aligned} \tag{8}$$

3. Optimization Results

The optimization problem was carried out for a rectangular wing with span length $R = 5$cm and chord length

Table 1
The quasi-steady aerodynamic model developed by Wang et al [8] was used to extract the lift and drag forces acting on a flapping wing executing a harmonic sweeping motion. The time-normalized angular acceleration at various instances of the stroke are also listed.

Stroke Phase	Aerodynamic Force (N)	Angular Acceleration ($\mathrm{rad\,s^{-2}}$)
Mid- upstroke	0.0331	0.0000
End- upstroke	0.0028	-41.3417
Transition (up- to down- stroke)	0.0172	-29.2329

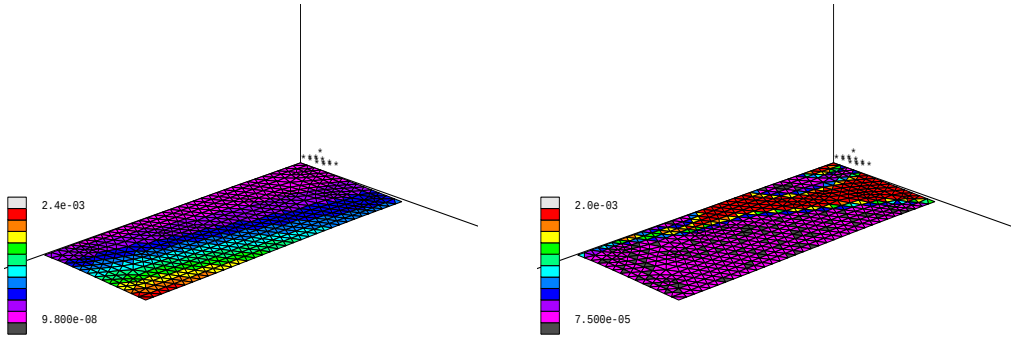

(a) Average Displacement [m] plot of the obtained design. (b) Thickness distribution [m] plot of the obtained wing design.

Figure 2: Optimization results obtained for the mid-upstroke phase are shown in the figures, under only aerodynamic load. Axis lines show the origin of the global coordinate system, and the clamping boundary condition for $C = 0$ to $C = 0.004$m is shown with the help of asterisks. It can be seen here that the design does not obtain the required angle of attack.

$C = 2$cm. PETG was chosen as the material, with Young's modulus $E = 3$GPa and density $\rho = 1200\mathrm{kg\,m^{-3}}$. The maximum wing thickness was set to 2 mm and the minimum thickness was set to 75 µm. The results for different phases of the flapping stroke are shown in Fig 2 to 4. Note that all the figures plot the deformed configuration of the wing under the specified load case.

Fig 2 shows the design obtained by the wing for the mid-upstroke phase of the flapping stroke. It can be seen that design obtained from optimization does not achieve the required angle of attack at the wing tip. This is to be expected for the case where only the aerodynamic load acts, as the centre of pressure of the load is very close to the pitching axis of the wing. One must also keep in mind that the wing enters this phase of the stroke already possessing a certain angle of attack due to the transient inertial forces in the phases leading up to this instant. The low magnitude of the load does not generate enough moment to allow a rotation about the pitching axis in a quasi-static situation. The displacement plot shows that the optimizer has arranged material so as to form a sort of compliant mechanical hinge near the clamped region.

Fig 3 and 4 show the thickness distributions obtained by the optimizer for two different phases of the upstroke where the inertial load is dominant as compared to the aerodynamic load. It can be seen that areas of large thickness, and therefore mass, near the clamped boundary helps increase bending stiffness of the wing. Inertial loads are dependent on the local mass of the structure and hence, the rest of the mass is concentrated along the trailing edge of the wing tending to higher concentrations towards the wing tip, allowing the structure to pitch. This is very similar to the function of the *pterostigma* [5] found in many insects.

Under purely inertial loads, the optimizer obtains a design which includes a small protrusion with high thickness near the wing's leading edge which can be seen in Fig 4. This addition could help in strengthening the bending stiffness of the structure. Note that certain low thickness regions of the obtained optimal design exhibit very low deflection near the wing root and then have larger deflections after a certain point when moving along the chord. This could be caused by the combination of the small added high thickness protrusion, and low inertial loads present near the wing root. This behavior can also be seen in Fig 3 for the load case with both aerodynamic and inertial loads, albeit in a more subtle manner. The stiffening behavior near the wing root for this case could be caused due to the high thickness distributions near the wing leading and trailing edges, leading to a very narrow channel with low thickness.

A similar optimization study was carried out for a hawk-moth wing shape with a smaller clamped region (2 mm of clamping) and the obtained results are shown in Fig 5 to 7. The bounds on thickness and the material parameters used are identical to the previous case with the simple rectangular wing planform. This study was done to understand the influence of wing planform shape on the overall obtained thickness distributions.

Reducing the clamped region and changing the wing shape

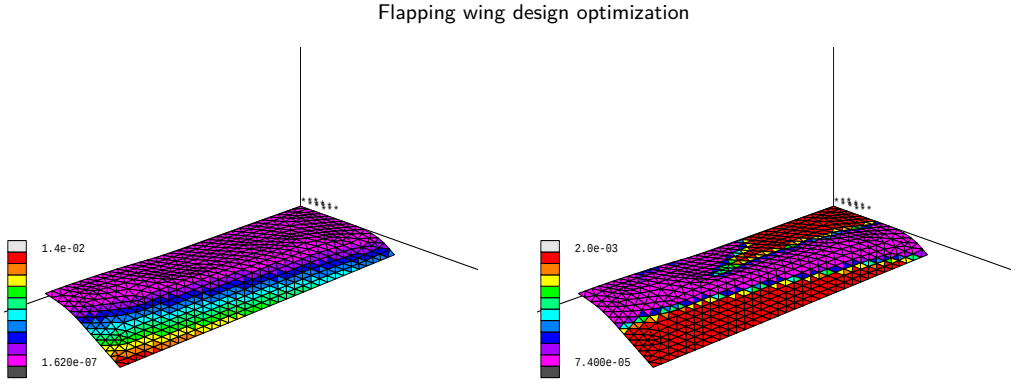

(a) Average Displacement [m] plot of the obtained design. (b) Thickness distribution [m] plot of the obtained wing design.

Figure 3: Optimization results obtained for the transition from up- to downstroke are shown in the figures, under both the inertial and aerodynamic loads. Axis lines show the origin of the global coordinate system, and the clamping boundary condition for $C = 0$ to $C = 0.004$m is shown with the help of asterisks. The obtained angle of attack is $40.18°$.

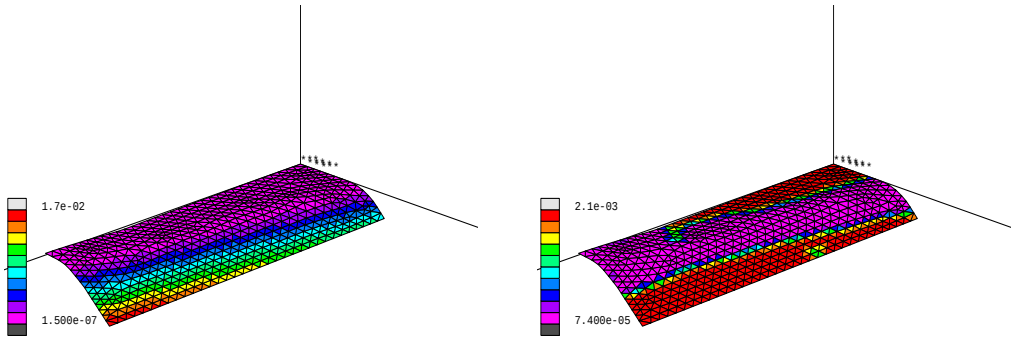

(a) Average Displacement [m] plot of the obtained design. (b) Thickness distribution [m] plot of the obtained wing design.

Figure 4: Optimization results obtained for the end of the upstroke are shown in the figures. The load case considers only the inertial load as the aerodynamic load has relatively much lower magnitude. Axis lines show the origin of the global coordinate system, and the clamping boundary condition for $C = 0$ to $C = 0.004$m is shown with the help of asterisks. The obtained angle of attack is $43.15°$, which is close to the lift-maximizing angle of attack required.

has some interesting effects. Although the optimizer's approach of concentrating some mass near the clamping and the rest near the trailing edge stays the same, there are some subtle changes to the obtained thickness distributions. For instance, the obtained designs for the mid-upstroke phase of both wing shapes show significant differences in the way the optimizer chooses to distribute thickness, and therefore, mass (see Fig 2 and 5). To understand why this difference occurs, plots of the membrane forces (given by the tangential stress resultants) and bending moments (given by the tangential stress couples) were studied. The bending moments were similar for both wing shapes but the membrane forces, shown in Fig 8, are different.

It can be seen from Fig 8 that there are areas with high membrane forces near the leading edge of the rectangular wing whereas these do not exit for the hawkmoth wing. Instead, one can see that most of the membrane forces act near the clamped region for the latter. This difference in membrane forces could arise due to the difference in clamped regions between the two wing cases, as the clamped region for the rectangular wing is larger and thus more restrictive. Another significant change that could be a cause of the variation in obtained designs is the load itself. Recall that the aerodynamic load also depends on the shape of the wing. The load centre of pressure is closer to mid-span for the hawkmoth wing, whereas for the rectangular wing it is closer to the wing tip. Indeed, neither of the designs can be called "feasible" for the mid-stroke phase without a more rigorous study on the shape-dependent aerodynamic load. However, as the magnitude of this load is not as large as the inertial load, there is merit to understanding obtained designs under the inertial load.

The designs obtained under dominating inertial loads are shown in Fig 6 and 7. Note that although the angle measured at a point 2 cm away from the wing tip is slightly lower than the required angle of attack, it is expected that under true transient loading, the angles achieved will be slightly higher. The patterns formed are very similar to those that were obtained for the rectangular wing. Under both aerodynamic and inertial loads, a protrusion similar to the one found in

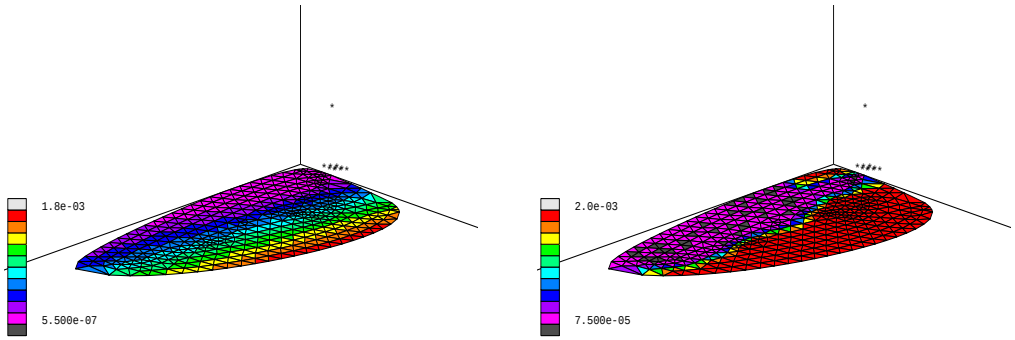

(a) Average Displacement [m] plot of the obtained design. (b) Thickness distribution [m] plot of the obtained wing design.

Figure 5: Optimization results obtained for the mid-upstroke phase of a hawkmoth wing are shown in the figures, under only aerodynamic load. Axis lines show the origin of the global coordinate system, and the clamping boundary condition is shown with the help of asterisks. It can be seen here that the design does not obtain the required angle of attack.

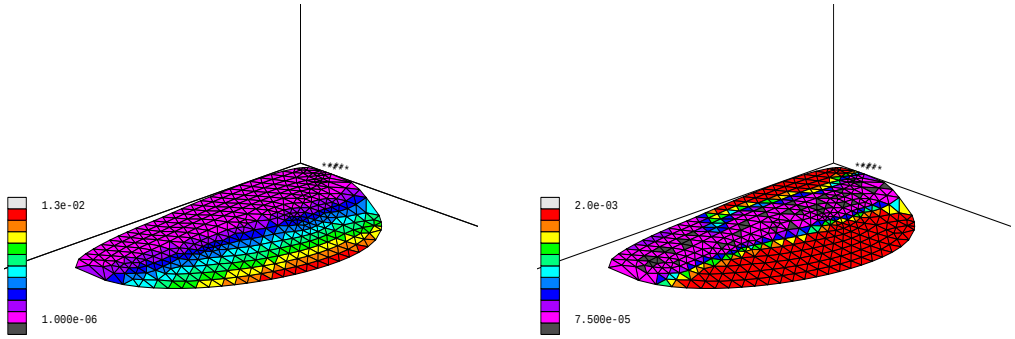

(a) Average Displacement [m] plot of the obtained design. (b) Thickness distribution [m] plot of the obtained wing design.

Figure 6: Results obtained for the transition from up- to downstroke of a hawkmoth wing are shown in the figures, under both the inertial and aerodynamic loads. Axis lines show the origin of the global coordinate system, and the clamping boundary condition is shown with the help of asterisks. The obtained angle of attack is 36.25° at a point on the trailing edge 2 cm away from the wing tip.

Fig 4 can be seen, although this is of a much more subtle nature. Since it is not as pronounced in this case, it does not provide as much stiffening at the wing root.

4. Summary and Conclusion

Wing design for application in a FWMAV is a highly nuanced topic with vast scope for future research. In order to obtain an optimized thickness distribution for the flapping wing under different load cases, a sensitivity implementation was developed that takes into account the difference in proportionality between membrane and bending stiffnesses, and also the dependence of inertial load on the design variable. Optimization results obtained for two wing planform shapes under various loads indicate a general thickness pattern that is required to achieve the design objectives. A tendency to concentrate thickness (and consequently, mass) near the clamped boundary and the wing trailing edge was observed for both wing shapes. Potential caveats with the designs obtained for the shape-dependent aerodynamic pressure load were identified and highlighted, and a possible explanation for the subtle variances in designs was discussed.

For future research, we would recommend a more rigorous formulation of the shape-dependent aerodynamic pressure load as it is important to the objective of achieving a truly accurate optimal design. The sensitivity of the pressure load to the deformation profile of the structure, and therefore implicitly, the design variable needs to be studied in depth and implemented. This would also help improve optimization convergence rates and increase the certainty of obtaining a feasible design.

References

[1] Dickinson, M.H., Lehmann, F., Sane, S.P., 1999. Wing rotation and the aerodynamic basis of flight. Science 284, 1954–1960.

[2] Ellington, C.P., van den Berg, C., Willmott, A.P., Thomas, A.L.R., 1996. Leading-edge vortices in insect flight. Nature 384, 626–630. URL: https://doi.org/10.1038/384626a0, doi:10.1038/384626a0.

[3] Floreano, D., Wood, R.J., 2015. Science, technology and the future

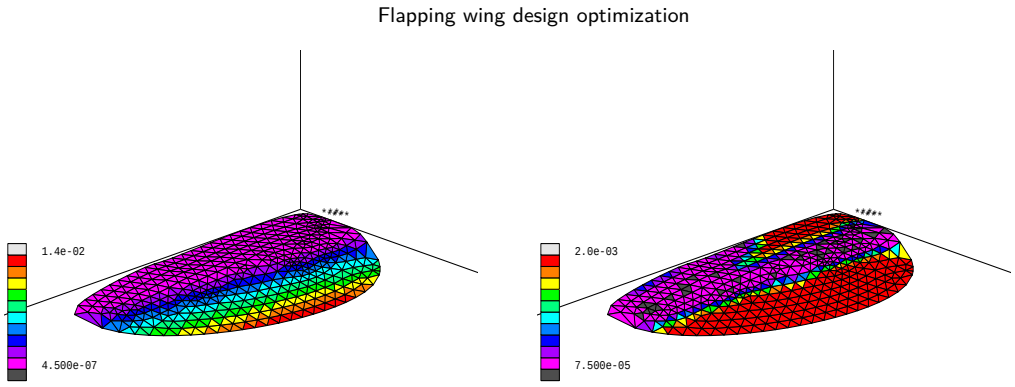

(a) Average Displacement [m] plot of the obtained design. (b) Thickness distribution [m] plot of the obtained wing design.

Figure 7: Results obtained for the end-upstroke phase of a hawkmoth wing are shown in the figures. This load case considers only the inertial load, which has a much higher magnitude than the aerodynamic load. Axis lines show the origin of the global coordinate system, and the clamping boundary condition is shown with the help of asterisks. The obtained angle of attack is 39.81° at a point on the trailing edge 2 cm away from the wing tip.

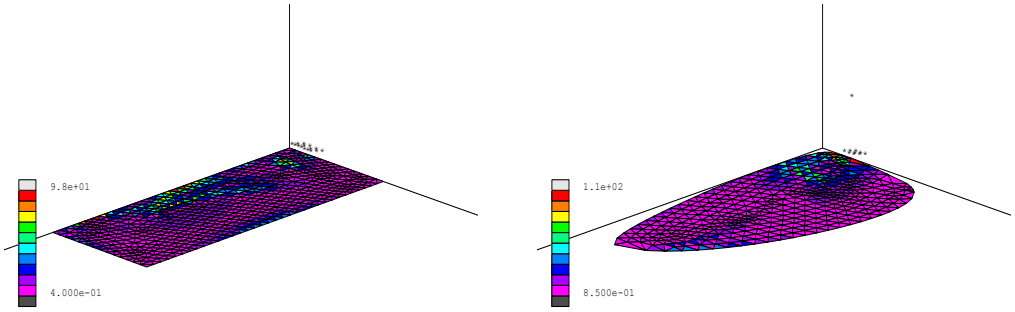

(a) Rectangular Wing Planform. (b) Hawkmoth Wing.

Figure 8: A comparison of the effective value of membrane forces for the rectangular and hawkmoth wing shapes. The effective value is calculated in a similar manner to the Von Mises stress.

of small autonomous drones. Nature 521, 460–466. doi:10.1038/nature14542, arXiv:arXiv:1011.1669v3.

[4] Liu, T., 2008. Comparative Scaling of Flapping- and Fixed-Wing Flyers. AIAA Journal 44, 24–33. doi:10.2514/1.4035.

[5] Norberg, R.Å., 1972. The pterostigma of insect wings an inertial regulator of wing pitch. Journal of comparative physiology 81, 9–22.

[6] Usherwood, J.R., Ellington, C.P., 2002. The aerodynamics of revolving wings I. Model hawkmoth wings. Journal of Experimental Biology 205, 1547 LP – 1564. URL: http://jeb.biologists.org/content/205/11/1547.abstract.

[7] Van Keulen, F., Booij, J., 1996. Refined Consistent Formulation of a Curved Triangular Finite Rotation Shell Element. International Journal for Numerical Methods in Engineering 39, 2803–2820. URL: https://doi.org/10.1002/(SICI)1097-0207(19960830)39:16{%}3C2803::AID-NME977{%}3E3.0.COhttp://2-2, doi:10.1002/(SICI)1097-0207(19960830)39:16<2803::AID-NME977>3.0.CO;2-2.

[8] Wang, Q., Goosen, J.F., Van Keulen, F., 2016. A predictive quasi-steady model of aerodynamic loads on flapping wings. Journal of Fluid Mechanics 800, 688–719. doi:10.1017/jfm.2016.413.

A. Appendix I - Sensitivity Verification

The symmetric plate approach discussed in Sec 2.1.2 was implemented in research code Charles developed by Van Keulen et al [7] and tested under various load cases. A triangular plate, modelled with just one CTRIB3 element was subjected to various loading conditions and the tangential stress couples and resultants were used to calculate the sensitivity of compliance with respect to the pseudo-thickness variable s_e described in previous sections.

Using the chain rule, it is known that

$$\frac{dC}{ds_e} = \frac{dC}{dt_e}\frac{dt_e}{ds_e}$$

$$\implies \frac{dC}{ds_e} = \frac{dC}{dt_e}t^0$$

With the above equation, a number of load tests were run and the sensitivity calculated by the optimizer was compared with sensitivities calculated manually. The results of these comparisons are viewable in Tables 2 to 6.

B. Appendix II - Pressure / Surface Load Implementation

The CTRIB3 element developed by Van Keulen et al [7] has already been implemented in the research code, Charles.

Table 2
Test 1 - Membrane Test. A distributed force of 100 N/m was applied in the X-direction on the hypotenuse of the triangular plate. An average displacement of 1.011e-08 m was observed. Sensitivity calculated by the optimizer was -1.516666529e-06. Sensitivity was manually calculated to be -1.516664926e-06. SI Units are used for all measures.

	t^0 = 1.000000e-02	$t^0 + \Delta t$ = 1.000001e-02
N_{xx}	6.4999998028333e+01	6.4999998028335e+01
N_{yy}	6.4999998028333e+01	6.4999998028335e+01
N_{xy}	3.4999998938333e+01	3.4999998938334e+01
M_{xx}	0.0000000000000e+00	0.0000000000000e+00
M_{yy}	0.0000000000000e+00	0.0000000000000e+00
M_{xy}	0.0000000000000e+00	0.0000000000000e+00
γ_{xx}	1.5166666206611e-08	1.5166651039961e-08
γ_{yy}	1.5166666206611e-08	1.5166651039961e-08
γ_{xy}	3.0333332413222e-08	3.0333302079921e-08
κ_{xx}	0.0000000000000e+00	0.0000000000000e+00
κ_{yy}	0.0000000000000e+00	0.0000000000000e+00
κ_{xy}	0.0000000000000e+00	0.0000000000000e+00

Table 3
Test 2 - Bending Test. A concentrated force of 1 N was applied on the vertex connecting sides 1 and 2. An average displacement of 1.099e-05 m was observed. Sensitivity calculated by the optimizer was -9.899999978e-05. Sensitivity was manually calculated to be -9.899998245e-05. SI Units are used for all measures.

	t^0 = 1.000000e-02	$t^0 + \Delta t$ = 1.0000001e-02
N_{xx}	4.2899999968562e-05	4.2899987099095e-05
N_{yy}	4.2899999968562e-05	4.2899987099095e-05
N_{xy}	2.3099999983072e-05	2.3099993053359e-05
M_{xx}	-9.9999999945552e-01	-9.9999999945552e-01
M_{yy}	-2.9161858113487e-16	7.4666214082698e-17
M_{xy}	-4.9999999972776e-01	-4.9999999972776e-01
γ_{xx}	1.0009999992664e-14	1.0009995988789e-14
γ_{yy}	1.0009999992664e-14	1.0009995988789e-14
γ_{xy}	2.0019999985329e-14	2.0019991977579e-14
κ_{xx}	-3.9999999978221e-05	-3.9999987978223e-05
κ_{yy}	1.1999999993466e-05	1.1999996393467e-05
κ_{xy}	-5.1999999971687e-05	-5.1999984371690e-05

Table 4
Test 3 - Bending Test. A moment of 10 N.m was applied on side 2. An average displacement of 2.333e-05 m was observed. Sensitivity calculated by the optimizer was -9.899999999e-03. Sensitivity was manually calculated to be -9.899998256e-03. SI Units are used for all measures.

	t^0 = 1.000000e-02	$t^0 + \Delta t$ = 1.0000001e-02
N_{xx}	1.9293595407977e-08	1.9293573315573e-08
N_{yy}	1.9294473492012e-08	1.9294451399696e-08
N_{xy}	1.0389095473074e-08	1.0389083577188e-08
M_{xx}	-6.1246461818598e-09	-6.1246397268864e-09
M_{yy}	1.0000000000000e+01	1.0000000000000e+01
M_{xy}	4.9999999969377e+00	4.9999999969377e+00
γ_{xx}	4.5017511201246e-18	4.5017455150469e-18
γ_{yy}	4.5021316232063e-18	4.5021260181287e-18
γ_{xy}	9.0038827433309e-18	9.0038715331757e-18
κ_{xx}	-1.2000000024499e-04	-1.1999996424499e-04
κ_{yy}	4.0000000007350e-04	3.9999988007352e-04
κ_{xy}	5.1999999968152e-04	5.1999984368155e-04

Table 5
Test 4 - Membrane and Bending Test. Concentrated forces of 1 N in X- and Z- directions were applied on vertex connecting sides 1 and 2. An average displacement of 1.099e-05 m was observed. Sensitivity calculated by the optimizer was -9.899080634e-05. Sensitivity was manually calculated to be -9.898752084e-05. SI Units are used for all measures.

	t^0 = 1.000000e-02	$t^0 + \Delta t$ = 1.0000001e-02
N_{xx}	1.3000428970878e+00	1.3000428970750e+00
N_{yy}	1.3000428970878e+00	1.3000428970750e+00
N_{xy}	7.0002309843190e-01	7.0002309842497e-01
M_{xx}	-9.9996700115117e-01	-9.9996700116107e-01
M_{yy}	1.1368683772162e-16	-3.1500734252177e-17
M_{xy}	-4.9998350057559e-01	-4.9998350058054e-01
γ_{xx}	3.0334334265382e-10	3.0334331231649e-10
γ_{yy}	3.0334334265382e-10	3.0334331231649e-10
γ_{xy}	6.0668668530765e-10	6.0668662463298e-10
κ_{xx}	-3.9998680046047e-05	-3.9998668046841e-05
κ_{yy}	1.1999604013814e-05	1.1999600414052e-05
κ_{xy}	-5.1998284059861e-05	-5.1998268460894e-05

Table 6
Test 5 - Membrane and Bending Test. Concentrated forces of 10 kN in X- direction and 1 N in Z-direction were applied on vertex connecting sides 1 and 2. An average displacement of 8.514e-06 m was observed. Sensitivity calculated by the optimizer was -6.070764392e-02. Sensitivity was manually calculated to be -6.069336724e-02. SI Units are used for all measures.

	t^0 = 1.0000000e-02	$t^0 + \Delta t$ = 1.00000001e-02
N_{xx}	1.2999921162783e+04	1.2999921162784e+04
N_{yy}	1.2999921162783e+04	1.2999921162784e+04
N_{xy}	6.9999575491910e+03	6.9999575491914e+03
M_{xx}	-7.5188312863449e-01	-7.5188313423121e-01
M_{yy}	0.0000000000000e+00	0.0000000000000e+00
M_{xy}	-3.7594156431725e-01	-3.7594156711560e-01
γ_{xx}	3.0333149379828e-06	3.0333149076498e-06
γ_{yy}	3.0333149379828e-06	3.0333149076498e-06
γ_{xy}	6.0666298759655e-06	6.0666298152996e-06
κ_{xx}	-3.0075325145380e-05	-3.0075324466989e-05
κ_{yy}	9.0225975436139e-06	9.0225973400966e-06
κ_{xy}	-3.9097922688994e-05	-3.9097921807085e-05

However, existing functionality only allowed for uniform pressure loadings. The slender and highly nonlinear nature of the flapping wing problem made the response of the system highly sensitive to changes in the net force applied. Hence, an approximate modelling of the load distribution was deemed to be insufficient.

In order to calculate the work equivalent nodal forces, there were two approaches available. The first approach is to manually carry out the integration and then evaluate the integral at different points to obtain nodal forces for each element. Say the pressure distribution is given by some $q(x, y)$, and the shape functions for the element are denoted by the $\mathbf{N}$-vector. The nodal forces for each element can be calculated by the following equation.

$$\int_A \mathbf{N}^T q(x, y) \; dA$$

Since the equation of the cubic surface is of order 3 in both, the $x-$ and $y-$ directions, the above equation is basically integration of a fourth order equation with multiple coefficients. Doing such an integration by hand was deemed to be a difficult endeavour and hence, a Gaussian integration scheme using linear shape functions was set up.

The position of any point $P(x_P, y_P)$ in a triangle can be defined by using the areal or triangular coordinate system. Point P can then be described using the ratio of the area of the sub-triangles to the area of the whole triangle. Looking at Fig 9, we can define shape functions for each point as the ratio of these areas such that

$$P(x_P, y_P) = \begin{bmatrix} \xi_1 & \xi_2 & \xi_3 \end{bmatrix}$$

where $\xi_i = \frac{A_i}{A}$.
If we now consider an isosceles right triangle such as

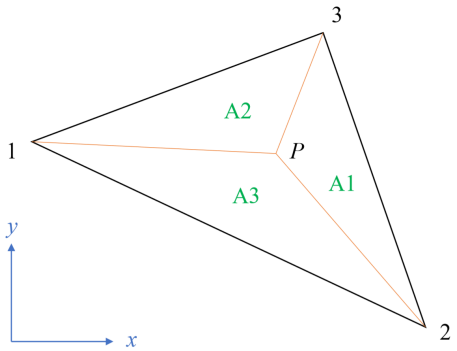

Figure 9: Any point $P(x_P, y_P)$ in a triangle can be represented using areal coordinates as shown. The ratio of the area of the sub-triangles to the area of the whole triangle gives information on the location of point P.

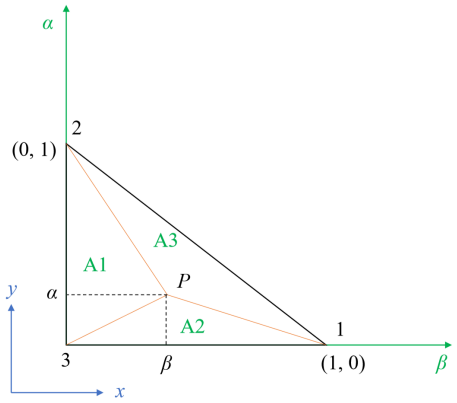

Figure 10: Point $P(x_P, y_P)$ in a triangle can be represented using local coordinates derived from the areal coordinates.

shown in Fig 10, we can calculate the ratio of the areas as shown below.

$$\xi_1 = \frac{A_1}{A} = \frac{\frac{1}{2} \times 1 \times \alpha}{\frac{1}{2} \times 1 \times 1} = \alpha$$

$$\xi_2 = \frac{A_2}{A} = \frac{\frac{1}{2} \times 1 \times \beta}{\frac{1}{2} \times 1 \times 1} = \beta$$

$$\xi_3 = \frac{A - A_1 - A_2}{A} = 1 - \alpha - \beta$$

These are the linear shape functions for a triangular element. Following this, a simple numerical integration scheme was implemented in order to calculate the exact nodal forces that each element experiences. The exact integral was converted to the numerical integral as shown below.

$$\int_A \mathbf{N}^T q(x, y) \; dA = \sum_i^{n_{GP}} \mathbf{N}^T q(\alpha_i^{-1}, \beta_i^{-1}) w_i j$$

In the above equation, n_{GP} is the number of Gauss integration points, j is the determinant of the Jacobian for the transformation from (x, y) to (α, β), and w_i is the weight assigned for each Gauss point.

Chapter 5

Conclusion and Reflection

In conclusion, the research questions that were established after the literature review portion of this project have been answered. Key parameters that influence lift generation characteristics of a wing were defined. Different portions of the flapping stroke were studied and crucial parts were identified. During the mid-stroke phase, the wing experiences very little forces due to inertia. As a result, only the aerodynamic pressure load acts perpendicular to the wing surface at that instant. The inherent nature of selecting snapshots of the stroke and running quasi-static analyses is that information pertaining to the transients, such as the angle of attack at the wing tip as the wing enters the mid-stroke phase, is lost. The aerodynamic centre of pressure being in close proximity to the pitching axis means that not enough torque is generated to allow the wing to pitch passively under quasi-static conditions. The transition phase, which marks the change in motion from upstroke to downstroke is also of high importance because the wing experiences a combined loading from the aerodynamic pressure and the inertial surface load. For wings that pitch passively, the inertial load is generally significantly higher and hence, obtained optimized designs reflect this difference in magnitudes. Optimal designs for this load case are quite similar to the designs obtained for the end-stroke phase, where inertial loads dominate compared to the relatively negligible aerodynamic loads.

Of particular interest are tiny protrusions or appendices of high mass concentration near the wing leading edge in the optimal designs. These structures tend to strengthen bending stiffness at the wing tip but also have the parasitic effect of increasing stiffness at the wing root. These stiffening structures are very similar to the venations found in real insect wings which perform a similar function. Another interesting pattern observed was the tendency of the optimizer to concentrate mass close to the wing trailing edge, increasing somewhat linearly from the wing root to the wing tip. These thick regions experience a higher local inertial load and generate a significant moment about the pitching axis to achieve the required angle of attack. This is also found in nature in the form of the *pterostigma*, which is thought to assist in wing pitching in insects.

A short supplementary study was carried out to investigate the effects of initial values given to the design variable. For the hawkmoth shape wing under purely inertial loads, two cases

were compared - one where the optimization was started with a uniform low thickness, and another where it was started with a uniform high thickness. The obtained final designs for each case are shown in Fig 5-1. Although both the obtained results deform in a very similar manner, it can be seen that there are some differences in the obtained distributions. A corresponding plot of the membrane forces acting on the final designs are shown in Fig 5-2, and once more, differences can be easily observed. This seems to indicate that for the currently defined optimization problem, there exist more than one so-called "optimal" solution. This would make sense from a realistic standpoint as the currently defined problem covers a vast majority of wing designs found to occur naturally. To obtain a more specific design, a more narrow formulation of the optimization problem may be required and hence, a more intense study on this is necessary to draw any firm conclusions.

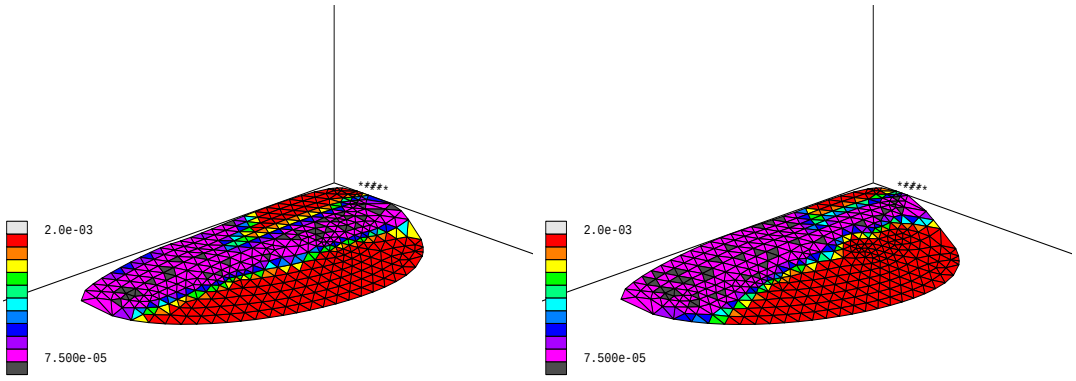

(a) Obtained design for low initial thickness **(b)** Obtained design for high initial thickness

Figure 5-1: Thickness distributions obtained for two cases of initial thickness are shown here. Although unintentional, the design corresponding to high initial thickness (b) seems to exhibit higher displacements close to the wing root. This may be due to the reduced amount of material concentration near the clamped region.

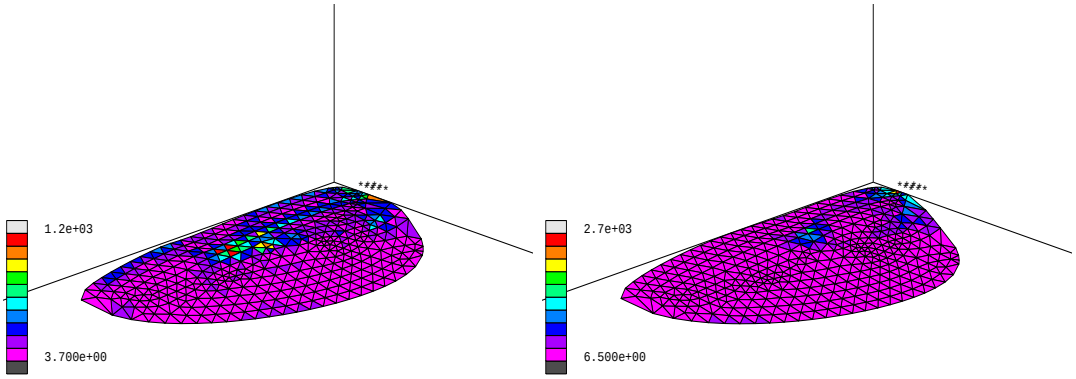

(a) Obtained design for low initial thickness **(b)** Obtained design for high initial thickness

Figure 5-2: Membrane forces (calculated in a Von Mises way) for the obtained optimal designs corresponding to cases of initial thickness are shown here. It can be seen that the latter case (b) has forces of larger magnitude near the clamped region.

A few caveats need to be reiterated such as the missing sensitivity terms that describe the explicit dependency of the pressure load on the deformation of the wing itself, and thus also

the implicit dependency of the same load on the thickness distribution of the wing. This is a complicated topic that requires further research. Additionally, although an approximate representation of the aerodynamic load at mid-stroke was developed in the form of a cubic load distribution, the changing profile of the aerodynamic load throughout the stroke and its dependency on the shape of the wing planform was not implemented accurately. This was done because the dominance of the inertial loads leads to the straightforward assumption that these would be the limiting case. For instance, a wing that is stiff under only the lower magnitude aerodynamic load need not necessarily possess a large enough stiffness to withstand the high inertial loads at different parts of the stroke. Nevertheless, a more rigorous implementation would be interesting in terms of further study.

In terms of future research and other approaches, there are a multitude of options other than implementing the caveats mentioned in the previous paragraph. One possibility is to formulate an objective function that incorporates multiple load cases by means of assigning weights to each load case or by some other kind of min-max formulation. Including a large enough number of load cases could potentially result in a design that acts as a sort of global optimum for the flapping wing use case. Another option would be to try and come up with venation-like structures similar to those found on insect wings. This could be done by choosing a compliant base material such as PETG and another material with higher stiffness. With an upper limit on the volume of the stiffer material, one could try to come up with a distribution of this stiffer material on the surface of the base material such that the entire combined structure exhibits certain desired characteristics. There are also practical research projects that involve manufacturing obtained optimal designs and testing them on an apparatus that generates the required sweeping motion. This would be useful to see how well the designs obtained from quasi-static analyses translate to an actual scenario where the wing experiences a large amount of transient forces. All of these projects would form a natural extension to this thesis project and are avenues worth exploring to solidify understanding of the fundamental design of wings for flapping wing flight.

Bibliography

[1] T. Liu, "Comparative Scaling of Flapping- and Fixed-Wing Flyers," *AIAA Journal*, vol. 44, no. 1, pp. 24–33, 2008.

[2] Q. Wang, J. F. L. Goosen, and F. van Keulen, "An efficient fluidstructure interaction model for optimizing twistable flapping wings," *Journal of Fluids and Structures*, vol. 73, pp. 82–99, 2017.

[3] B. J. Goodheart, "Tracing the History of the Ornithopter: Past, Present, and Future," *Journal of Aviation/Aerospace Education & Research*, vol. 21, no. 1, pp. 31–44, 2011.

[4] B. Kulfan, "Dr. John McMasters: following the foot steps of a creative paleoaerodynamicist," in *47th AIAA Aerospace Sciences Meeting including The New Horizons Forum and Aerospace Exposition*, p. 869, 2009.

[5] A. Berget, *The Conquest of the Air, Aeronautics, Aviation, History: Theory: Practice*. GP Putnam's sons, 1911.

[6] Z. J. Jackowski, "Design and construction of an autonomous ornithopter," 2009.

[7] R. J. Wood, "The first takeoff of a biologically inspired at-scale robotic insect," *IEEE transactions on robotics*, vol. 24, no. 2, pp. 341–347, 2008.

[8] G. De Croon, K. M. E. De Clercq, R. Ruijsink, B. Remes, and C. De Wagter, "Design, aerodynamics, and vision-based control of the DelFly," *International Journal of Micro Air Vehicles*, vol. 1, no. 2, pp. 71–97, 2009.

[9] D. Floreano and R. J. Wood, "Science, technology and the future of small autonomous drones," *Nature*, vol. 521, no. 7553, pp. 460–466, 2015.

[10] C. P. Ellington, C. van den Berg, A. P. Willmott, and A. L. R. Thomas, "Leading-edge vortices in insect flight," *Nature*, vol. 384, no. 6610, pp. 626–630, 1996.

[11] M. H. Dickinson, F. Lehmann, and S. P. Sane, "Wing rotation and the aerodynamic basis of flight," *Science*, vol. 284, no. June, pp. 1954–1960, 1999.

[12] J. R. Usherwood and C. P. Ellington, "The aerodynamics of revolving wings I. Model hawkmoth wings," *Journal of Experimental Biology*, vol. 205, pp. 1547 LP – 1564, jun 2002.

[13] U. Pesavento and Z. J. Wang, "Flapping wing flight can save aerodynamic power compared to steady flight," *Physical Review Letters*, vol. 103, no. 11, pp. 1–4, 2009.

[14] Weis-fogh and B. Y. Torkel, "Fitness in Hovering Animals , Including Novel Mechanisms for Lift Production," *Journal of Experimental Biology*, vol. 59, no. 1, pp. 169–230, 1973.

[15] C. T. Bolsman, *Flapping wing actuation using resonant compliant mechanisms.* 2010.

[16] T. van Wageningen, "Design analysis for a small scale hydrogen peroxide powered engine for a flapping wing mechanism micro air vehicle," 2012.

[17] A. Selvan, "Simulation of optic flow based flight control for a flapping wing micro aerial vehicle," 2014.

[18] H. J. Peters, J. F. L. Goosen, and F. van Keulen, "Methods to actively modify the dynamic response of cm-scale FWMAV designs," *Smart Materials and Structures*, vol. 25, no. 5, p. 55027, 2016.

[19] Q. Wang, J. F. L. Goosen, and F. Van Keulen, "A predictive quasi-steady model of aerodynamic loads on flapping wings," *Journal of Fluid Mechanics*, vol. 800, pp. 688–719, 2016.

[20] F.-O. Lehmann and S. Pick, "The aerodynamic benefit of wingwing interaction depends on stroke trajectory in flapping insect wings," *Journal of experimental biology*, vol. 210, no. 8, pp. 1362–1377, 2007.

[21] S. P. Sane, "The aerodynamics of insect flight," *Journal of experimental biology*, vol. 206, no. 23, pp. 4191–4208, 2003.

[22] S. P. Sane and M. H. Dickinson, "The aerodynamic effects of wing rotation and a revised quasi-steady model of flapping flight," *Journal of Experimental Biology*, vol. 205, pp. 1087 LP – 1096, apr 2002.

[23] C. P. Ellington, "The aerodynamics of hovering insect flight. II. Morphological parameters," *Philosophical Transactions of the Royal Society of London. B, Biological Sciences*, vol. 305, no. 1122, pp. 17–40, 1984.

[24] S. P. Sane and M. H. Dickinson, "The control of flight force by a flapping wing: lift and drag production," *Journal of experimental biology*, vol. 204, no. 15, pp. 2607–2626, 2001.

[25] R. Å. Norberg, "The pterostigma of insect wings an inertial regulator of wing pitch," *Journal of comparative physiology*, vol. 81, no. 1, pp. 9–22, 1972.

[26] A. J. Bergou, S. Xu, and Z. J. Wang, "Passive wing pitch reversal in insect flight," *Journal of Fluid Mechanics*, vol. 591, pp. 321–337, 2007.

[27] J. P. Whitney and R. J. Wood, "Aeromechanics of passive rotation in flapping flight," *Journal of fluid mechanics*, vol. 660, pp. 197–220, 2010.

[28] S. A. Ansari, R. Żbikowski, and K. Knowles, "Aerodynamic modelling of insect-like flapping flight for micro air vehicles," *Progress in aerospace sciences*, vol. 42, no. 2, pp. 129–172, 2006.

[29] O. Sigmund, "A 99 line topology optimization code written in Matlab," *Structural and multidisciplinary optimization*, vol. 21, no. 2, pp. 120–127, 2001.

Glossary

FWMAV	Flapping Wing Micro Air Vehicle
MAV	Micro Air Vehicle
SWAD	Spanwise Area Distribution
CWAD	Chordwise Area Distribution
SWMD	Spanwise Mass Distribution
CWMD	Chordwise Mass Distribution
PA	Pitching Axis
AoA	Angle of Attack